

AD P 001925

EFFECT OF DEFECTS ON AIRCRAFT COMPOSITE STRUCTURES

by

R. A. Garrett

Branch Chief, Technology

McDonnell Aircraft Company

P. O. Box 516, St. Louis, Missouri 63166

USA

SUMMARY

This paper describes the effects of manufacturing and service-induced damage on the static and fatigue strength of aircraft composite structures.

Seven manufacturing defects associated with mechanical fasteners were investigated; out-of-round holes, broken fibers on the exit side of drilled holes, porosity, improper fastener seating depth, tilted countersinks, interference fit, and multiple fastener installation and removal cycles. Both static and fatigue test results are described, along with correlation with analysis techniques. The interaction of the effects of these defects on hole wear, measured in fatigue tests of structural joints, is described.

The effects of two types of service-induced damage are also described; low energy impact damage and 23mm HEI ballistic damage. The relative sizes of visible and non-visible damage as determined by visual and non-destructive inspection techniques are compared. An evaluation of stitching and the inclusion of glass or Kevlar fiber buffer strips to improve the damage tolerance of carbon/epoxy structures is included. Results of tests of carbon/epoxy panel structures are discussed. Correlation of experimental results with predicted residual static strength is good.

LIST OF SYMBOLS

- C - compression
- d - diameter
- e - edge distance
- E_a^b - extensional modulus measured in the "a" direction due to "b" loading
- ETW - elevated temperature test with prior specimen moisture conditioning
- σ_{bru} - ultimate failing bearing stress
- G - shear modulus
- LEID - low energy impact damage
- N - number of fatigue cycles
- NDI - nondestructive inspection
- N_{xy} - shear load intensity
- N_{xy}^{cr} - shear load intensity at initial buckling
- R - fatigue load ratio; minimum load divided by maximum load
- RT - room temperature
- RTD - room temperature test with no specimen moisture conditioning
- RTW - room temperature test with specimen moisture conditioning
- T - tension
- w - specimen width
- ϵ_a^b - strain measured in the "a" direction due to "b" loading
- ϵ^u - ultimate failing strain
- AS/3501-6 (typ.) - material system nomenclature for type AS carbon fibers in a 3501-6 epoxy resin matrix
- 50/40/10 - laminate nomenclature in which the three numbers describe the percent of plies oriented in the 0°, +45° and 90° directions, respectively; i.e., 50% of total number of plies are oriented in the 0° direction, 40% of the plies are oriented in the +45 directions and 10% of the plies are oriented in the 90° direction.

1. INTRODUCTION AND BACKGROUND

Future aircraft will require airframes that are lighter weight, easier to maintain and more durable than current construction approaches and materials. The use of composite materials in primary structures offers promise of significant weight savings, due to their greater specific static strength and even larger improvement in fatigue strength. However, proof of the ability of composite structures to be tolerant of both initial manufacturing defects and damage induced by service usage was necessary before their application to aircraft primary structures.

Programs to evaluate the damage tolerance of composite structures have been initiated by several different agencies under the Department of Defense. Each of these programs have been directed towards a different aspect of the subject area; this paper summarizes some of the work performed by the McDonnell Aircraft Company in each area.

The effect of manufacturing defects on the static and fatigue strength of laminates with loaded and unloaded fastener holes was conducted in Reference (1) program and is described in Section 2. The effect of low energy impact damage on composite structures was included in several programs with the United States Navy (References 2, 3, and 4); the results are described in Section 3. Finally, the effect of ballistic damage caused by 23 mm high-explosive projectiles conducted in conjunction with Reference (2) program is described in Section 4.

2. MANUFACTURING DEFECTS AT FASTENER HOLES

The effects of several types of manufacturing defects commonly found in aircraft structures were investigated under Reference (1) program. This investigation was performed using laminates with loaded fastener holes, a common critical structural design feature in aircraft composite structures. In many cases, tests were conducted with specimens in which the defect or anomaly was more severe than expected from current manufacturing processes. In all cases, defects which resulted in strength reductions greater than 15% would have been detected using current industry inspection techniques and would have been rejected or repaired to meet current acceptance criteria.

Tests were performed to determine the effects on static strength, compared to baseline specimens, and the effects on fatigue strength and hole wear.

(a) Static Strength - The effect of seven manufacturing defects on static strength was evaluated by comparing static strength of joints with a particular defect with the static strength of baseline joint specimens with no defect. The test matrix is presented in Figure 1.

Anomaly	Number of Tests Per Environment			Total Specimen Tests
	RT (Dry) Tension	RT (Wet) Compression	ET (Wet) Compression	
1 Out of Round Holes				
"1" Laminate (50/40/10)	4	-	-	4
"2" Laminate (30/60/10)	4	-	-	4
2 Broken Fibers on Exit Side of Hole				
Severe Delamination	4	4	4	12
Moderate Delamination	4	4	4	12
3 Porosity around hole				
Severe Porosity	4	2,2 \triangle	4	12
Moderate Porosity	-	2,2 \triangle	4	8
4 Improper Fastener Seating Depth				
80% of Thickness	4	-	-	4
100% of Thickness	4	-	-	4
5 Tilted Countersinks				
Away from Bearing Surface	4	-	4	8
Toward Bearing Surface	4	-	4	8
6 Interference Fit	Layup			
0.003 In.	1	4	4 \triangle	8
	2	4	4	8
0.008 In.	1	4	4	8
	2	4	4	8
7 Fastener Removal and Reinstallation				
100 Cycles	4	-	4	8
Total				116

\triangle After freeze thaw cycling \triangle Tension tests

CP330117-28

Figure 1. Evaluation of Manufacturing Anomalies - Test Matrix

Specimens were tested to failure in tension and compression at three environmental conditions: room temperature dry (RTD), room temperature wet (RTW), and elevated temperature wet (ETW). ETW tests were conducted at 250°F with specimen moisture contents of approximately .80 percent by weight. Hercules AS/3501-6 carbon/epoxy was used for fabrication of test specimens.

Results from tests are summarized in Figure 2. Indicated percentages of increased or decreased strength are based on a comparison with baseline specimens. Detailed results are discussed below.

	RTD TENSION	COMPRESSION	
		RT Δ	250°F Δ
OUT-OF-ROUND HOLES • 50/40/10 LAMINATE • 30/60/10 LAMINATE	• -4.8	- -	- -
BROKEN FIBERS EXIT SIDE OF HOLE • SEVERE • MODERATE	-7.3 -1.4	-8.4 -3.2	-9.2 -4.2
POROSITY AROUND HOLE • SEVERE • SEVERE WITH FREEZE-THAW • MODERATE • MODERATE WITH FREEZE-THAW	• - - -	-10.3 -11.6 -7.1 -8.4	-30.8 - -13.3 -
IMPROPER FASTENER SEATING DEPTH • 80% THICKNESS • 100% THICKNESS	-16.4 -34.3	- -	- -
TILTED COUNTERSINKS • AWAY FROM BEARING SURFACE • TOWARD BEARING SURFACE	• -21.4	- -	-16.7 -16.7
INTERFERENCE FIT TOLERANCES (INCH) • 50/40/10 @ 0.003 @ 0.008 • 30/60/10 @ 0.003 @ 0.008	• • • •	- - - -	+9.1 Δ +9.1 Δ • •
FASTENER REMOVAL AND REINSTALLATION • 100 CYCLES	•	-	-8.3

Δ 0.86% moisture content Δ Tensile loading *Less than 2% change - No test

GP1340115-100

Figure 2. Strength Reduction Summary

Out of Round Holes - Effects of out-of-round holes on joint strength were evaluated by drilling offset (.004 inch) holes as shown in Figure 3. Test results of specimens from two laminates (50/40/10 and 30/60/10, where 90°plies/45°plies/90°plies are denoted in that order) indicated little sensitivity to out-of-round holes.

Broken Fibers on Exit Side of Hole - Specimens were tested for two conditions; "moderate" delaminations and "severe" delaminations. In order to obtain the various degrees of delamination, drill procedures included use of dull bits without backup material, and improper drill and feed speeds.

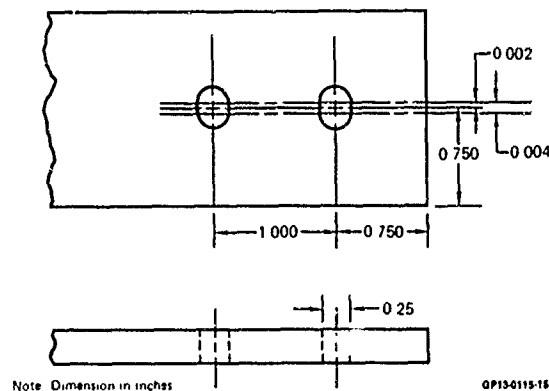


Figure 3. Out-of-Round Holes - Specimen

Delaminations were detected visually and with ultrasonic C-scan. Delaminations were defined as "moderate" when they extended 10-20 percent (2-4 plies deep) into the laminate thickness on the exit side. Delaminations were defined as "severe" when they extended 20-30 percent (4-6 plies) of the laminate thickness on the exit side. Non-destructive C-scans in the area of the fastener holes with moderate and with severe delaminations are illustrated in Figure 4 and compared with a nominal condition.

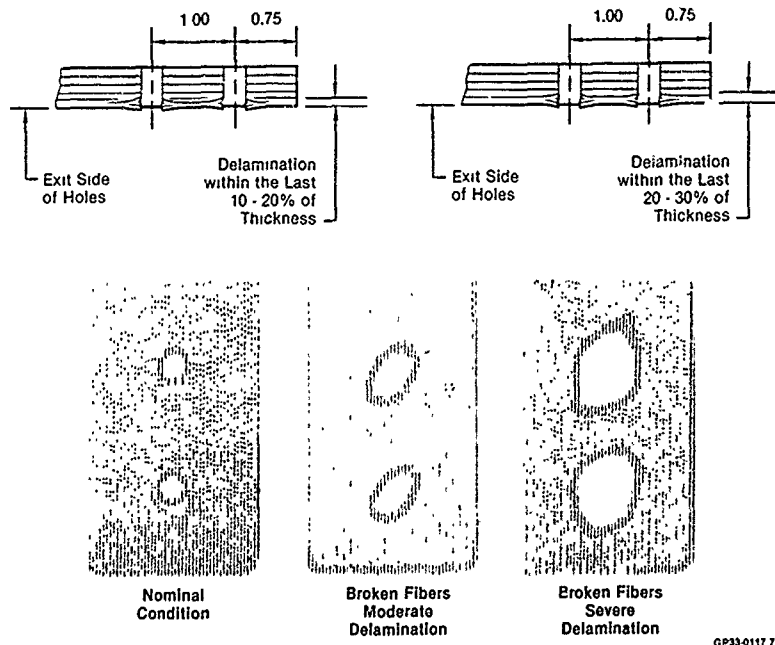
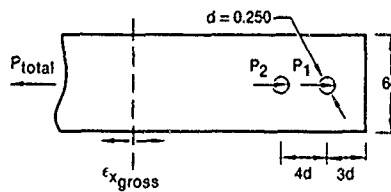


Figure 4. C-Scans of Laminates with Delaminations at Fastener Holes

Joint tension strength was evaluated by tests of dry laminates at room temperature. Because of its sensitivity to environment, joint compression strengths were evaluated at RTW and ETW test conditions.

Test results are summarized in Figure 5 along with baseline strength data. Strength reductions of 1.4 percent and 7.3 percent occurred in RTD tension tests for specimens with moderate and severe delaminations, respectively. Severe delaminations caused a 9.2% reduction of compression strength at 250°F.



Test Condition (50/40/10 Layout)	Baseline Data		Specimens with Delaminations		% Change		Loading
	$F_{x_2}^{bru}$ (ksi)	$\epsilon_{x_{gross}}^u$ ($\mu in./in.$)	$F_{x_2}^{bru}$ (ksi)	$\epsilon_{x_{gross}}^u$ ($\mu in./in.$)	F^{bru}	ϵ_{gross}	
RTD RTW ETW	+140 -155 -120	+3,990 -4,740 -3,790	Moderate		-1.4 -3.2 -4.2	-4.9 -6.2 +0.6	Ten Comp Comp
			+138	+3,790			
			-150	-4,450			
RTD RTW ETW	+140 -155 -120	+3,990 -4,740 -3,790	Severe		-7.3 -8.4 -9.2	-9.5 -3.5 -12.2	Ten Comp Comp
			+130	+3,610			
			-142	-4,580			
			-109	-3,330			

GP33-0117 5

Figure 5. Effect of Delaminations on Joint Strength

Porosity - Two levels of porosity were evaluated; "moderate" and "severe". Desired levels of porosity in the 50/40/10 laminate were obtained by using the altered collation and curing procedures summarized in Figure 6. Specimens were located within panels such that fastener holes occurred in areas of desired porosity levels as indicated by photomicrograph and nondestructive inspections (Figure 7).

Curing Procedure	Process Used for Good Panels	Process Used to Produce	
		Moderate Porosity	Severe Porosity
Vacuum Debulk	Yes	None	None
Intermediate Temperature Hold	1 hr @ 275°F	None	None
Bag Vacuum	0.05 in. Hg	0.8 in Hg	15 in Hg
Autoclave Pressure	100 psig	50 psig	50 psig
Add Moisture Δ	None	Every 7th Ply	Every Ply

Δ Fine mist sprayed between plies

GP33-0117-27

Figure 6. Panel Fabrication Procedures Used to Produce Panel Porosity

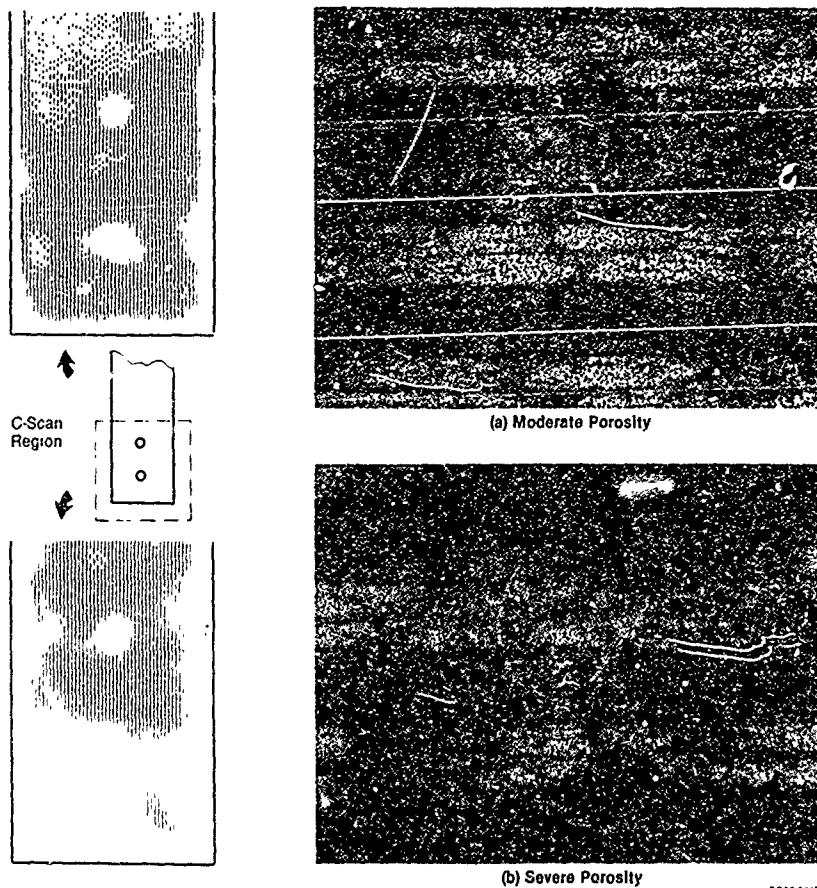


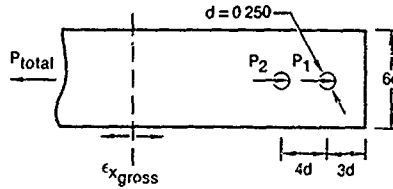
Figure 7. Examples of Panel Porosity

GP33-0117-4

Strengths of baseline specimens and specimens with porosity are compared in Figure 8. Little sensitivity to severe porosity was indicated under tensile loading. Under compressive loadings, strength reductions ranged from 7-13.3 percent for specimens with moderate porosity and 10-30.8 percent for specimens with severe porosity. The greatest reductions occurred at 250°F test condition.

Improper Fastener Seating Depth - Effects of excessive countersink depth on joint strength were evaluated by testing composite joint members having fasteners seated too deeply in a typical laminate (50/40/10). Two conditions of countersink depth were evaluated at room temperature in tension.

Strengths are compared with baseline strengths in Figure 9. Strengths for joints with excessive countersink depths (80% and 100%) are compared with strength of specimens with nominal countersink depths (52% of laminate thickness). Joint strengths for countersink versus noncountersink laminates indicated no significant reductions occurred when fastener seating depth was nominal. The relative amount of cylindrical bearing area as compared to countersink bearing area may account for the demonstrated loss in strength. Earlier tests have indicated that the maximum cylindrical bearing capacity is nearly 160 ksi for large edge distances. An analysis of the forces in the region of the countersink indicates an effective bearing capacity of 110 ksi, when friction is accounted for and when sufficient head bearing area still remains. Using these capacities results in predicted reductions of 14% and 30%, to be compared with the demonstrated reductions of 16.4% and 34.3%, respectively.

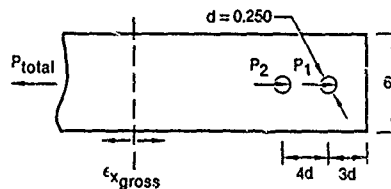


Test Condition (50/40/10 Layup)	Baseline Data		Specimens with Porosity		% Change		Loading
	F_{x2}^{bru} (ksi)	ϵ_{xgross}^u ($\mu\text{in./in.}$)	F_{x2}^{bru} (ksi)	ϵ_{xgross}^u ($\mu\text{in./in.}$)	F_{oru}	ϵ_{gross}	
			Moderate Porosity				
RTD	+140	+3,990	—	—	—	—	Ten
RTW	-155	-4,740	-144	-4,480	-7.1	-5.4	Comp
RTW (F-T) \triangle	-155	-4,740	-142	-4,370	-8.4	-7.9	Comp
ETW	-120	-3,790	-104	-3,110	-13.3	-17.9	Comp
			Severe Porosity				
RTD	+140	+3,990	+140	+3,940	0	-1.2	Ten
RTW	-155	-4,740	-139	-4,170	-10.3	-12.1	Comp
RTW (F-T) \triangle	-155	-4,740	-137	-4,110	-11.6	-13.3	Comp
ETW	-120	-3,790	-83	-2,550	-30.8	-32.6	Comp

\triangle (F-T) - exposed to freeze thaw cycles

GP33-0117-4

Figure 8. Effect of Porosity on Joint Strength



Countersink Depth (50/40/10 Layup) RTD, Tension	F_x^{bru} (ksi)	ϵ_{xGross}^u ($\mu\text{in./in.}$)	% Change	
			F_{bru}	ϵ_{Gross}
Nominal	140	3,990	—	—
80%	117	3,240	-16.4	-18.8
100% (Knife Edge)	92	2,540	-34.3	-36.3

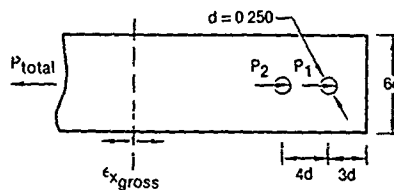
GP33-0117-3

Figure 9. Effect of Countersink Depth on Joint Strength

Tilted Countersinks - Countersink perpendicularity was investigated for two conditions of misalignment. The misaligned countersink was tilted 10° away from the bearing surface for one condition and tilted 10° toward it for the other. Tests were conducted in tension at RTD and in compression at 250°F after specimen moisture conditioning. Experimental results are summarized in Figure 10.

Interference Fit - The effects of fastener interference fits on joint strength were investigated in two different laminates (50/40/10 and 30/60/10). Two-fastener-in-tandem specimens were tested to failure in tension at RTD and ETW conditions. Specimens with both .003 and .008 inch levels of interference fit were tested.

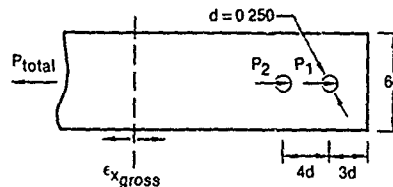
Results (Figure 11) for both layups indicate an insensitivity to interference at room temperature. Joint strength of the more fiber-dominant 50/40/10 layup improved under ETW conditions for both levels of interference. However, joint strengths of the matrix-dominant 30/60/10 layup showed no change at the ETW test condition.



Test Condition (50/40/10 Layup)	Baseline Data		Tilted Countersink		% Change		Loading
	f_{x2}^{bru} (ksi)	ϵ_{xGross}^u ($\mu\text{in./in.}$)	f_{x2}^{bru} (ksi)	ϵ_{xGross}^u ($\mu\text{in./in.}$)	f_{bru}	ϵ_{Gross}	
RTD ETW	+140 -120	+3,990 -3,750	Away From Bearing		0 -16.7	-2.0 -20.2	Ten Comp
			+140	+3,910			
RTD ETW	+140 -120	+3,990 -3,750	Toward Bearing		-21.4 -16.7	-24 -22.7	Ten Comp
			+110	+3,030			

GP330117-10

Figure 10. Effect of Tilted Countersink on Joint Strength



Test Condition	Baseline Data		Interference Fit		% Change		Loading		
	f_{x2}^{bru} (ksi)	ϵ_{xGross}^u ($\mu\text{in./in.}$)	f_{x2}^{bru} (ksi)	ϵ_{xGross}^u ($\mu\text{in./in.}$)	f_{bru}	ϵ_{Gross}			
50/40/10 Layup	140 110	3,990 3,080	0.003 Interference		0 +9.1	+0.4 +14.7	Ten Ten		
			140	4,000				120	3,530
			0.008 Interference					0 +9.1	+0.9 +11.2
			140	4,030					
30/30/10 Layup	140 120	5,470 4,710	0.003 Interference		0 0	-0.2 +2.4	Ten Ten		
			140	5,460				120	4,820
			0.008 Interference					0 0	+0.3 -1.8
			140	5,490					

GP330117-11

Figure 11. Effect of Fastener Interference Fit on Joint Strength

Laminate damage due to fastener installation at interference fits ranging from .002 to .008 inch were further evaluated for fasteners requiring pull-through installation techniques. Representative photomicrographs are shown in Figure 12. Little or no damage resulted from a fastener interference of .0035 inch or less; however, damage is indicated at the fastener exit side as well as along the entire fastener length for interference fits from .004 through .008 inch.

Fastener Removal and Reinstallation - These tests were used to evaluate whether repeated installation and reinstallation would locally damage the laminate hole area, and/or affect joint strength. Fasteners were installed, torqued to 50 inch-pounds, and completely removed. This procedure was repeated 100 times prior to strength testing. Specimens were tested to failure in tension at RTD and in compression at ETW.

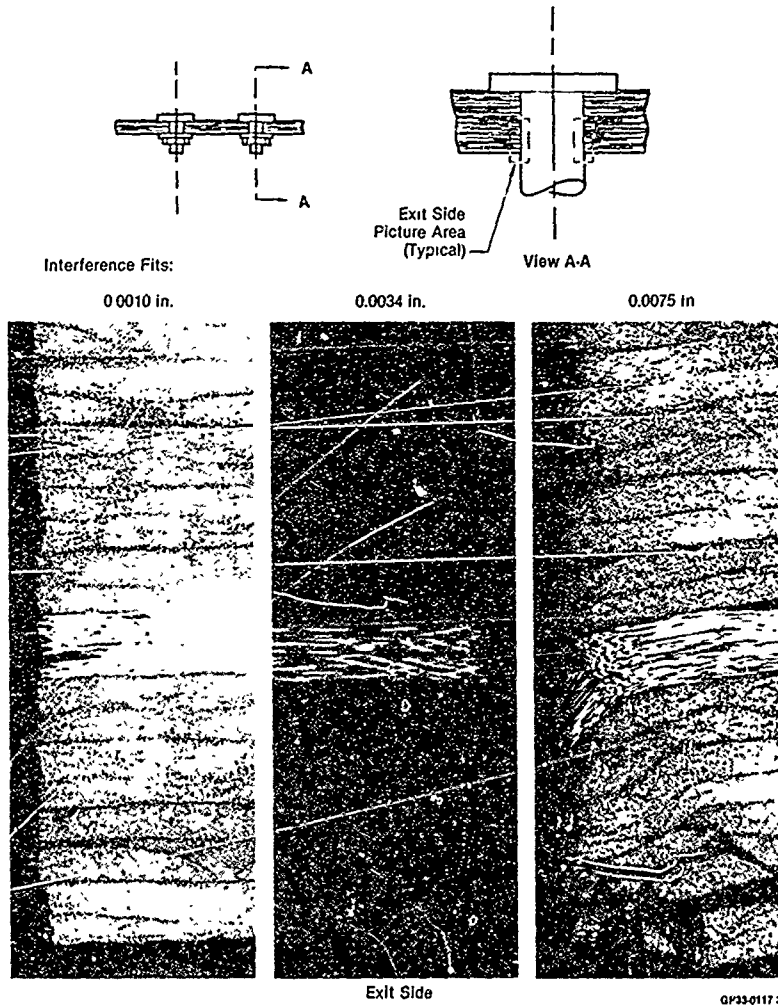


Figure 12. Photomicrograph Examination of Laminates with Interference Fit Holes

Visual appearance of all fastener holes after installation and re-installation cycling was unchanged. Strength data listed in Figure 13 indicates little sensitivity to RTD tensile test conditions. Compressive strength values indicated an increased sensitivity (8.3% reduction); however, test scatter for the compression tests was large.

(b) Fatigue Strength and Hole Wear - Tests were conducted with specimens with and without internal porosity to determine the effects on joint fatigue life, hole wear, and failure modes. Emphasis was placed on generation of hole wear data and its relation to joint fatigue life.

Test Condition (50/40/10 Layup)	Baseline Data		After 100 Cycles Fastener Installation		% Change		Loading
	$F_{x_2}^{bru}$ (ksi)	$\epsilon_{x_{gross}}^u$ ($\mu\text{in./in.}$)	$F_{x_2}^{bru}$ (ksi)	$\epsilon_{x_{gross}}^u$ ($\mu\text{in./in.}$)	F_{bru}	ϵ_{gross}	
RTD	+140	+3,990	+140	+3,900	0	-2.2	Ten
ETW	-120	-3,790	-110	-3,510	-8.3	-7.4	Comp

QP330117-13

Figure 13. Effect of Fastener Removal and Reinstallation on Joint Strength

A pure bearing test specimen was used (Figure 14). Tension-tension ($R = +0.1$) and tension-compression ($R = -1.0$) constant amplitude testing was performed at room temperature with specimens in the as-manufactured condition. Hercules AS/3501-6 carbon/epoxy was also used for fabrication of all fatigue and hole wear test specimens.

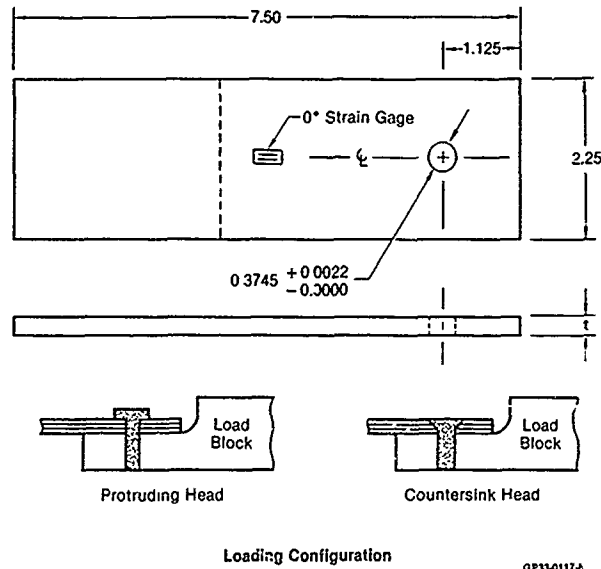


Figure 14. Fatigue Specimen Configuration

All constant-amplitude fatigue specimens were cycled to failure, or 10^6 cycles, whichever occurred first. Specimens which did not fail in 10^6 cycles were tested to determine residual strength. Constant amplitude fatigue testing was performed at three stress levels for each specimen type. Selection of the stress levels for fatigue testing was based on load-deflection data obtained from static tests. During fatigue testing, load-deflection data were also obtained each time a specified hole wear level was reached.

The evaluation included three layups; the fiber-dominated layup 50/40/10, and two matrix-dominated layups: 19/76/5 and 30/60/10.

Residual strengths were, in general, equal to or greater than nonfatigued specimen static strengths; however, in most cases, these specimens had acquired hole wear of .02 inch or greater during fatigue testing. For structural applications, hole elongations of .02 inch exceed the usual yield criteria for metallic joints which may also represent a tentative criteria for composite joints.

Results of tension-tension ($R = +0.1$) and tension-compression ($R = -1.0$) cyclic loading on each laminate at room temperature, dry (RTD) test conditions are summarized in Figures 15, 16, and 17, in terms of fatigue cycles required to produce an 0.02 inch hole wear in the fastener hole. The results indicate similar static and fatigue strength for all layups for tension-tension ($R = +0.1$) cycling, as summarized in Figure 18. For tension-compression ($R = -1.0$), the 19/76/5 and 30/60/10 matrix-dominant layups sustained fewer load cycles prior to developing an .02 inch hole wear, as compared to the 50/40/10 layup (Figure 19).

Tests of specimens with moderate porosity were conducted to evaluate the effects of this anomaly on joint durability. Earlier static tests indicated that moderate levels of porosity had a minor effect on static joint strength at room temperature. Specimens with moderate porosity in regions of fastener holes were tested under $R = +0.1$ and $R = -1.0$ fatigue loadings at room temperature dry conditions. Life data is compared in Figure 20 with baseline data. No reduction of static strength or joint fatigue life was indicated.

The rate of hole wear in other tests of composite joints without porosity at $R = +0.1$ is summarized in Figures 21, 22, and 23 for three levels of wear (.005, .010, and .020 inch). These data indicate that the matrix-dominant 19/76/5 layup exhibited earliest initiation of hole wear, but had the most gradual rate of accumulation. Conversely, the fiber-dominant (50/40/10) layup exhibited the most-delayed initiation of hole wear, but had the most rapid accumulation. The 30/60/10 layup exhibited an intermediate performance.

The spring rates of the test specimens for the 50/40/10 layup were also determined at various times in the constant amplitude fatigue testing to determine correlation with hole wear data. Hole wear data for this layup at RTD, shown in Figure 24 are similar in threshold points and trends to joint spring rate data summarized in Figure 25.

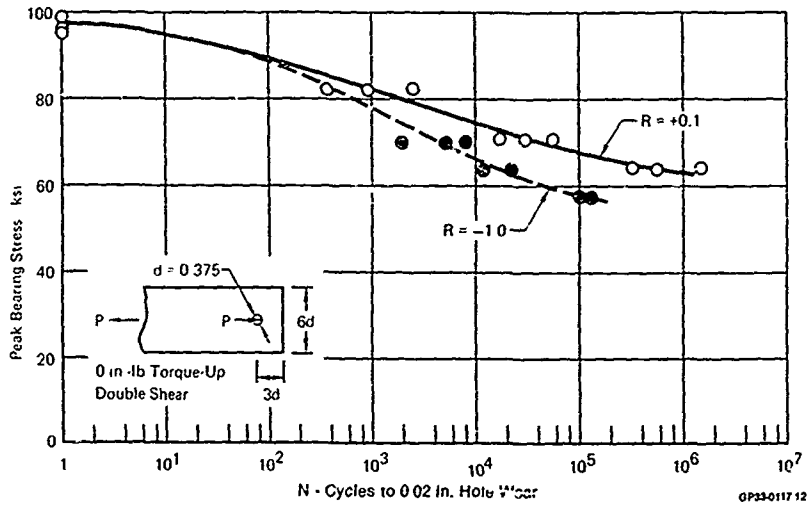


Figure 15. RTD Baseline Joint Fatigue Life
50/40/10 Layup

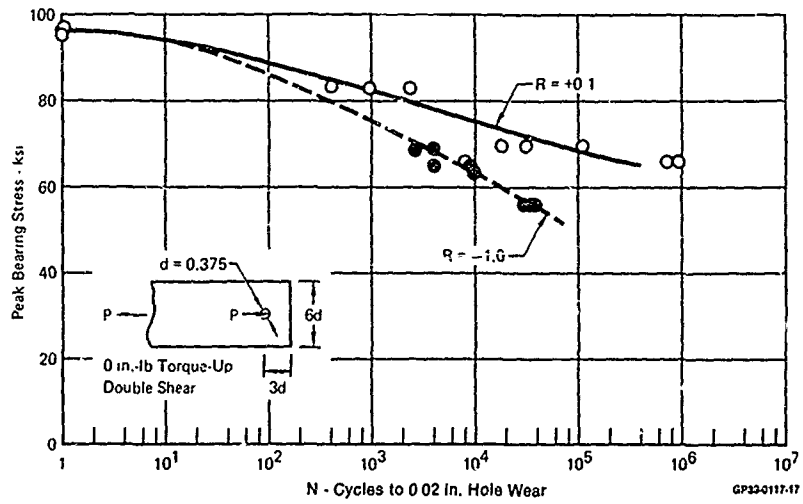


Figure 16. RTD Baseline Joint Fatigue Life
30/60/10

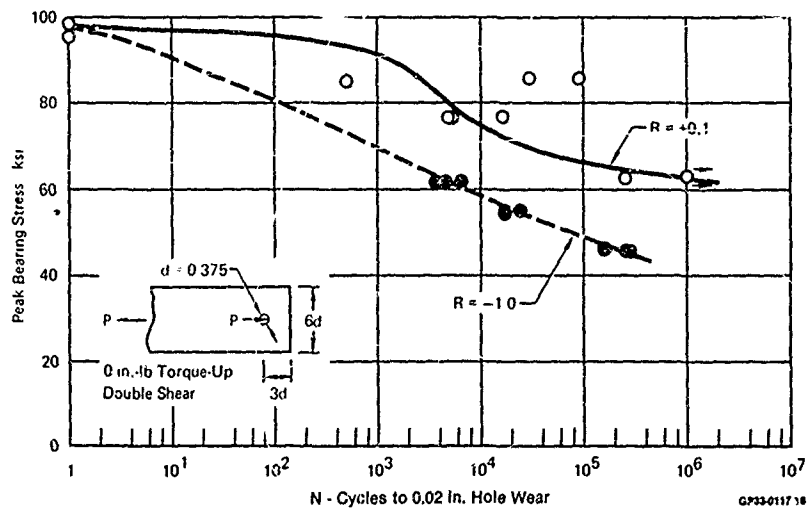


Figure 17. RTD Baseline Joint Fatigue Life
19/7/6/5 Layup

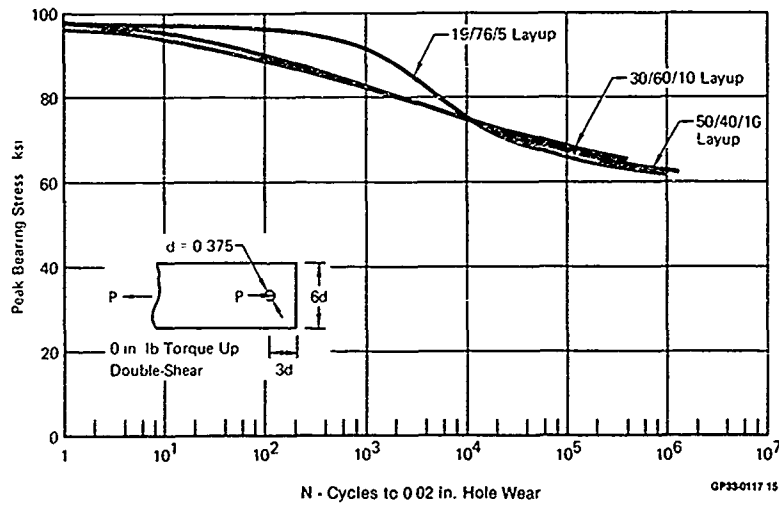


Figure 18. Comparison of $R = +0.1$ Joint Fatigue Life

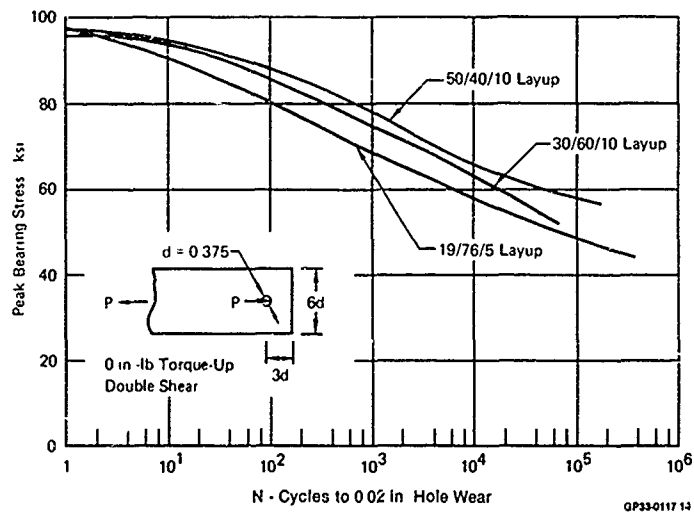


Figure 19. Comparison of $R = -1.0$ Joint Fatigue Life

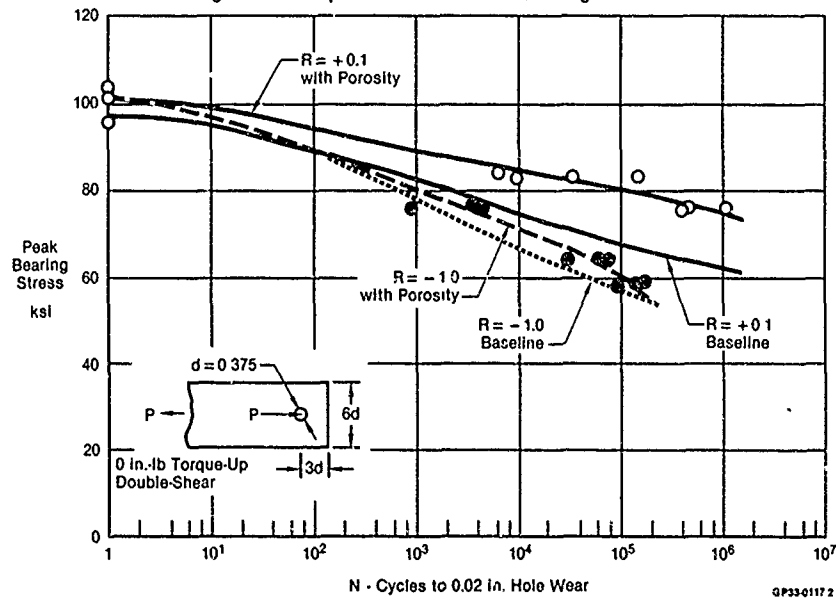


Figure 20. Effect of Porosity on Joint Fatigue Life
50/40/10 Layup

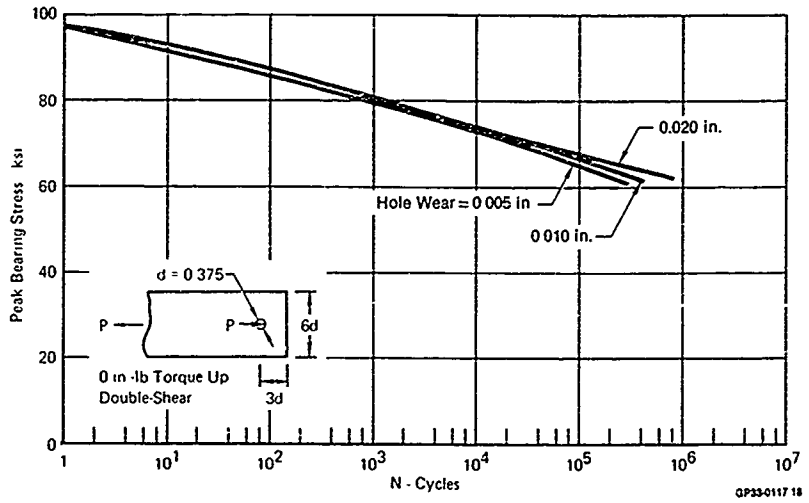


Figure 21. Hole Wear Under Fatigue Loading
50/40/10 Layup

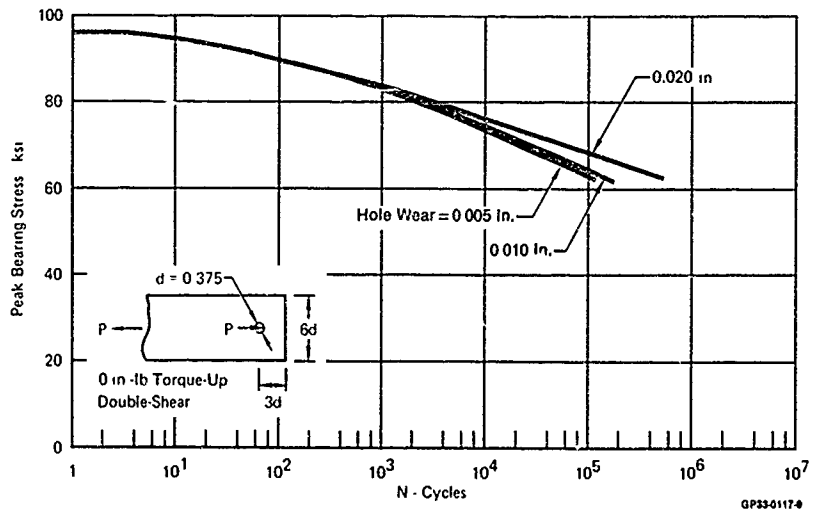


Figure 22. Hole Wear Under Fatigue Loading
30/80/10 Layup

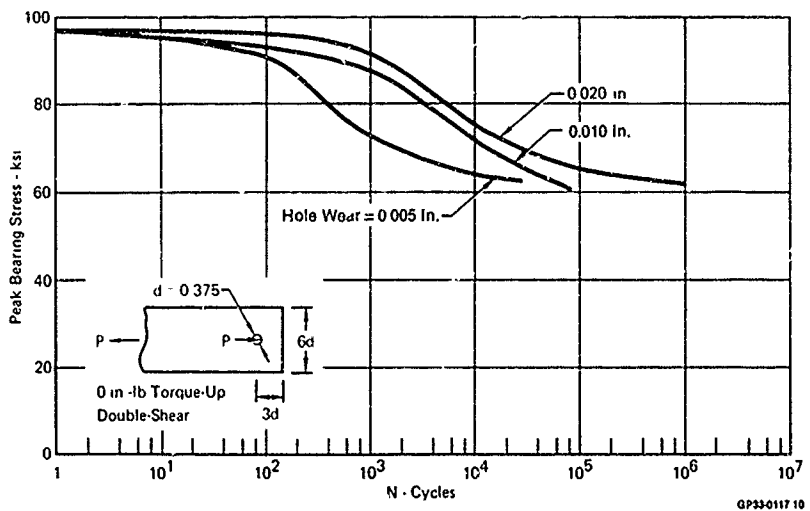


Figure 23. Hole Wear Under Fatigue Loading
19/76/5 Layup

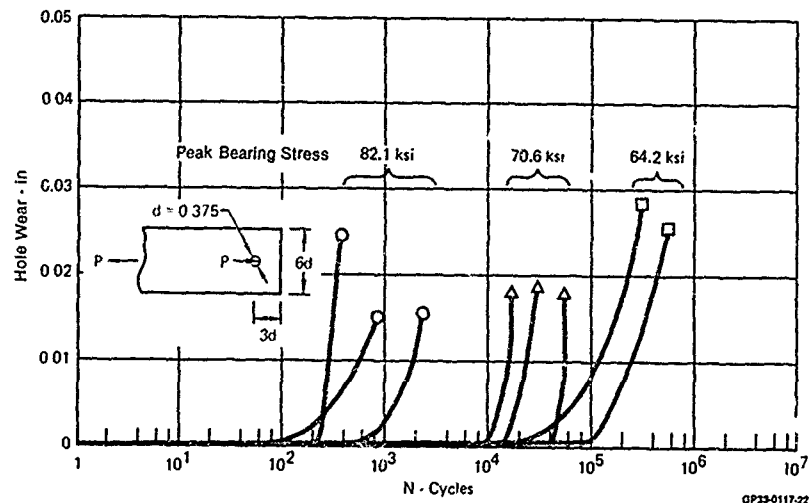


Figure 24. Effect of $R = +0.1$ Loading on Hole Wear
50/40/10 Layup

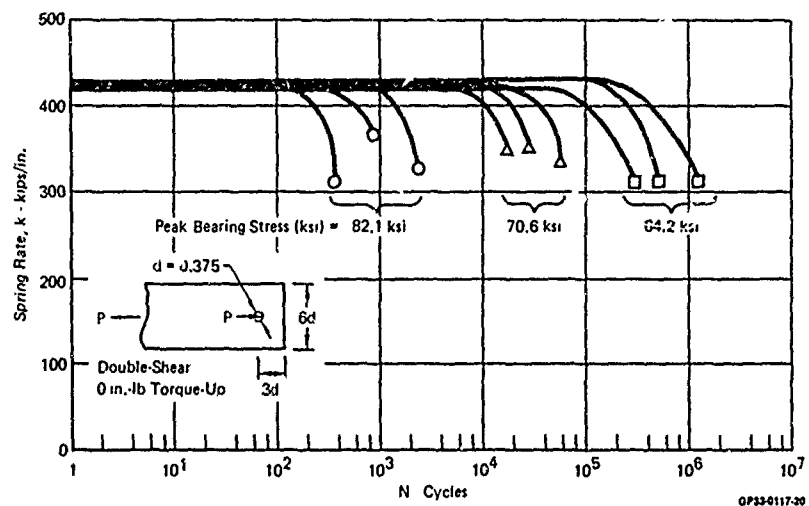


Figure 25. Effect of Fatigue Loading on Joint Spring Rate
50/40/10 Layup $R = +0.1$

3. LOW ENERGY IMPACT DAMAGE

The effect of low energy impact damage on the static and fatigue strength of carbon/epoxy wing cover skin structures and of integrally stiffened panels typical of postbuckling fuselage structures was evaluated.

(a) Wing Cover Skin Structural Panels - Effects of low-energy impact to an upper wing-skin were evaluated in static compression and fatigue tests (Reference 2). Specimens incorporated spanwise rows of Kevlar stitches simulating the patterns proposed for reinforcing cocured skin-to-stiffener joints.

The specimen configuration is presented in Figure 26. Various impact energies were evaluated to determine the energy level representing the threshold between visible and nonvisible impact damage. A .50-inch diameter indenter was used while specimens were supported over a 3-by-3-inch opening. An 8-ft-lb energy level was determined to be the minimum level to produce visible surface damage. The 8 ft-lb energy level was also considered to be representative of expected damage from dropped tools and damage from runway stones. Resulting internal damage detected in ultrasonic inspection of the four specimens ranged from 1.2-inch to 1.5-inch diameter.

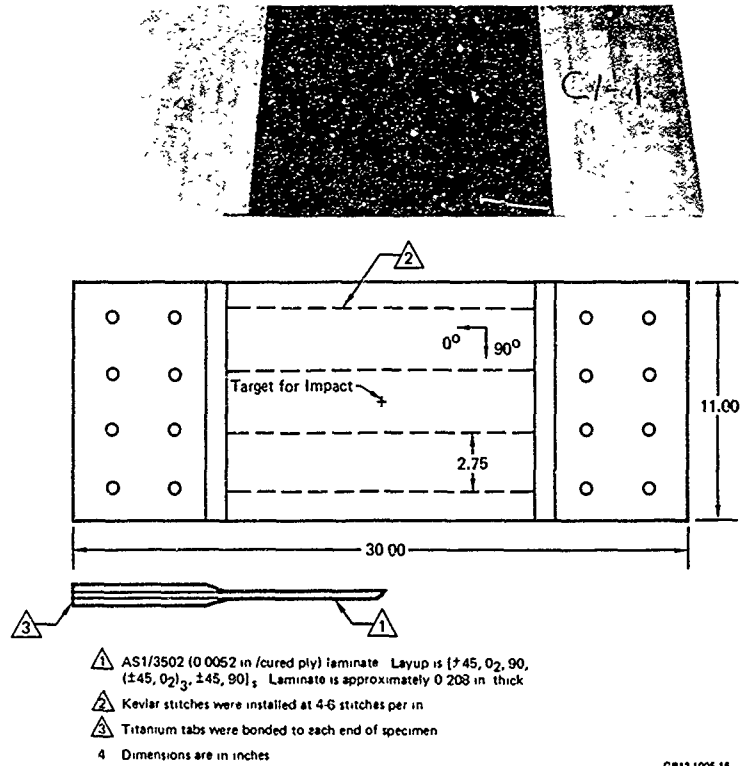


Figure 26. Specimen Configuration - Skins with Nonvisible Impact Damage

The setup for these compression tests is shown in Figure 27. Each end of the specimen was bolted to a loading adapter which fit within hydraulic grips in the upper and lower platens of the test machine. Back-to-back channels having access holes for instrumentation were clamped onto the specimen for skin stabilization. The area between the two central rows of stitches in the specimen contained the damage and was not stabilized by the channels. The column composed of the specimen with loading adapters on each end was supported at two locations by additional fixturing which was attached to the test machine. Strain data from back-to-back gages on the specimen indicated little bending. Measured strains in the stabilizing channels were negligible.

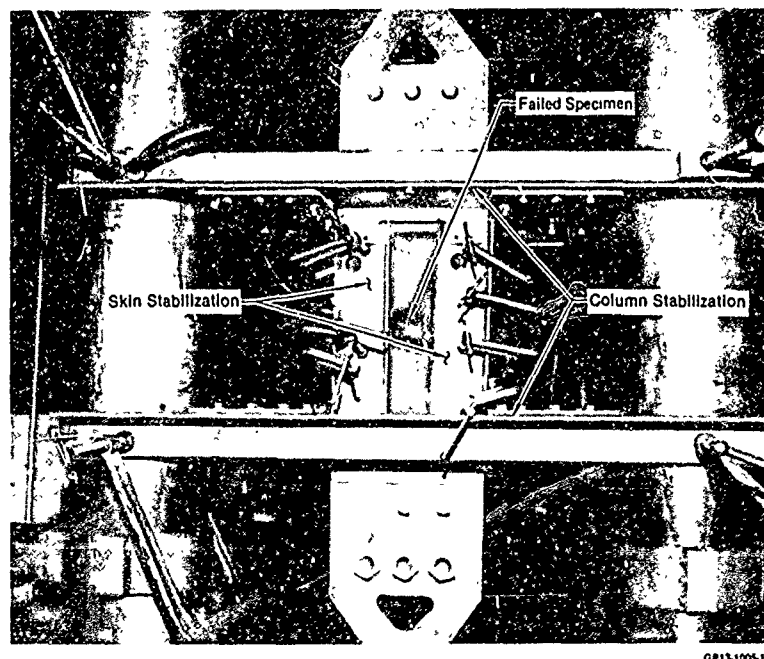


Figure 27. Structural Test Setup - Compressive Strength of Damaged Specimens

Results of static compression tests indicated that stitches were not sufficient to prevent damage propagation and overall failure at strain levels above $-4500 \mu\text{in/in}$. Strain data indicate local bending in the damaged area at low loads, possibly contributing to the failures.

A fatigue test of the remaining specimen was conducted to assess damage containment features of the stitch pattern. A compression-dominated spectrum was used. Damage detected in ultrasonic inspection was initially 1.6-inch long and 1.4-inch wide but grew to 1.7-inch long and 2.7-inch wide after 24,000 equivalent flight hours of spectrum loading. For the one specimen tested at the reduced strain level, damage was contained by parallel rows of stitches which were spaced at 2.75 in. In residual strength tests of this specimen, the far-field strain at failure was $-4200 \mu\text{in/in}$.

These test results are summarized in Figure 28 in terms of far-field failure strains as a function of damage sizes detected in ultrasonic inspections. Test results for coupons with a .25-inch diameter hole are also shown in Figure 28. The predicted strengths, presented as a solid line, were determined using the methodology of Reference 1 and the material properties shown in Figure 29. These predictions correlate well with test results for specimens having a .25-inch diameter hole. Predictions for specimens containing impact damage were made for damage modeled as open round holes.

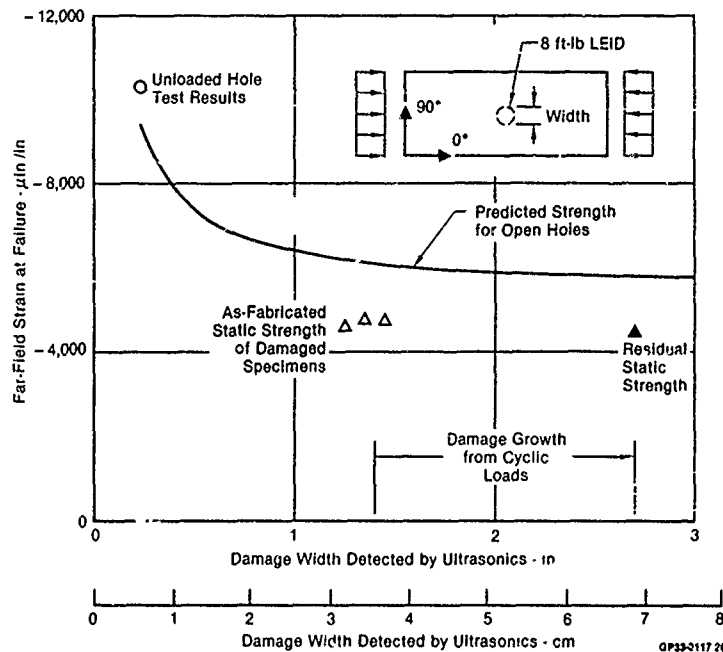


Figure 28. Residual Strength of Specimens with Nonvisible Impact Damage

Ply Property	Average Test (RTD)	
	AS1/2502	S-Glass/Epoxy*
E_1^T - psi (GPa)	18.3×10^6 (126.2)	8.0×10^6 (55.2)
E_1^C - psi (GPa)	17.3×10^6 (119.3)	7.5×10^6 (51.7)
E_2^T - psi (GPa)	1.4×10^6 (9.7)	2.7×10^6 (18.6)
E_2^C - psi (GPa)	1.8×10^6 (12.4)	2.7×10^6 (18.6)
G_{12} - psi (GPa)	0.9×10^6 (6.2)	0.8×10^6 (5.5)
ν_{12}	0.3	0.25
ϵ_1^T - $\mu\text{in/in}$	12,900	35,700
ϵ_1^C - $\mu\text{in/in}$	-18,200	-13,600
ϵ_2^T - $\mu\text{in/in}$	5,000	3,500
ϵ_2^C - $\mu\text{in/in}$	-26,500	-20,000
ϵ_{12} - $\mu\text{in/in}$	60,000	60,000

*Plastics for Aerospace Vehicles

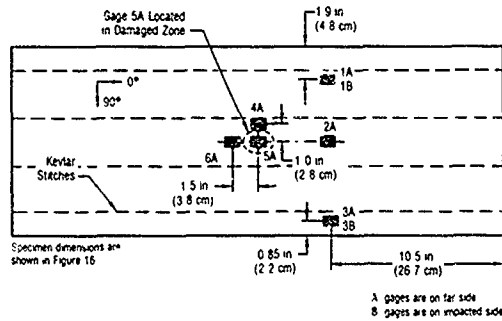
*Part 1 Reinforced Plastics, MIL-HDBK 17A, January 1971

GP33-0117 1

Figure 29. Composite Material Properties

Test results indicate that impact damage produced an effective strain concentration greater in magnitude than a round hole of equivalent size. Strengths predicted for an equivalent hole size were unconservative by approximately 30%, possibly due to local structural instability of delaminate plies within the damaged zone.

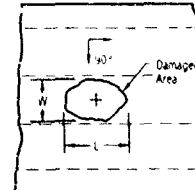
Test results are summarized in Figure 30, where strain data are shown for a nominal applied load of -20,000 lbs, the limit load level used for the fatigue test, and the failure load levels. Sizes of nonvisible impact damage were determined by ultrasonics and are also shown in this figure. A typical strength failure is shown in Figure 31. No fatigue failure occurred in four design lifetimes of spectrum fatigue loads.



Typical Strain Data Δ										
Event Δ	Load, kips (kN)	Specimen Number	Strain Gage Δ						6A	
			1A	1B	2A	3A	3B	4A	5A	
Low Load Strain Survey	-20 (-89)	C1 2	-809	-809	-952	-939	-976	-	-	-
		C1 3 (0 SFH) Δ	-684	-670	-914	-1 044	-1 027	-876	1 125	-921
		C1 3 (24k SFH)	-794	-785	-878	-930	-918	-866	F	-910
		C1 4	-713	-906	-838	-71	-775	-918	-1 119	-882
		C1 5	-936	-858	-860	-789	-77	-	-	-
Strains at Maximum Fatigue Load	-64.5 (-287)	C1 2	-2 916	-2 922	-3 063	-2 924	-3 010	-	-	-
		C1 3 (0 SFH)	-2 607	-2 532	-2 953	-3 262	-3 208	-3 092	-5 310	-3 096
		C1 3 (24k SFH)	-2 914	-2 874	-2 912	-2 957	-2 923	-2 658	F	-3 162
		C1 4	-2 346	-3 472	-2 571	-2 793	-2 688	-3 333	-5 544	-3 015
		C1 5	-3 248	-3 182	-2 209	-2 551	-2 471	-	-	-
Ultimate Strength	-100 (-446)	C1 2	-4 735	-4 728	-4 765	-4 651	-4 820	-	-	-
	-94 (-416)	C1 3 (24k SFH)	-	-	-	-	-	-	-	
	-100 (-466)	C1 4	-3 817	-4 276	-3 656	-4 493	-4 034	F	F	-4 524
	-96 (-426)	C1 5	-4 691	-4 606	F	-3 814	-3 746	-	-	-

Δ Strains are in units of $\mu\text{in/in}$
 Δ All tests conducted at room temperature
 Δ Specimen C1 3 tested in spectrum fatigue to an equivalent of 24 000 Spectrum Flight Hours (SFH)
 Δ Specimens C1 1 and C1 5 did not have strain gages 4A, 5A and 6A
 No ultimate strains recorded for specimen C1 3 because of instrumentation malfunction
 F = Gage failure

Size of Internal Damage Δ		
Specimen	L, in (cm)	W, in (cm)
C1 2	1.57 (3.99)	1.35 (3.42)
C1 3 (0 SFH)	1.57 (3.99)	1.36 (3.45)
C1 3 (24k SFH)	1.70 (4.32)	2.70 (6.86)
C1 4	1.79 (4.55)	1.43 (3.63)
C1 5	1.70 (4.32)	1.25 (3.18)



Δ Dimensions given are of internal damage
 L & W except where noted

GP13-1006-47

Figure 30. Residual Strength of Specimens with Nonvisible Impact Damage

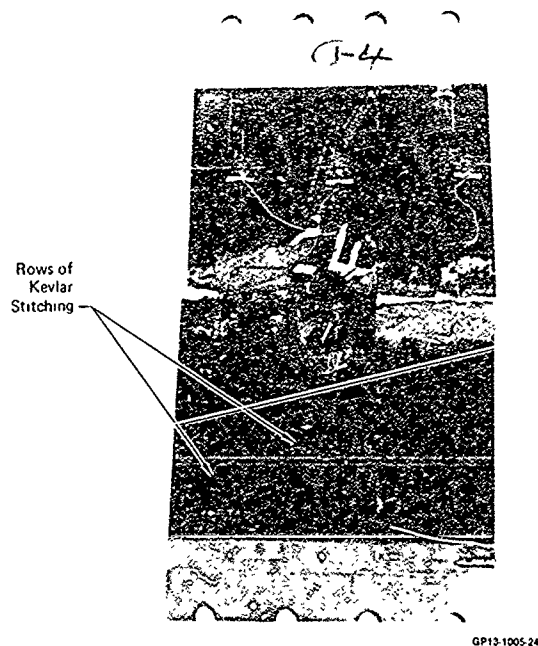


Figure 31. Typical Failed Skin Specimen

(b) Integrally Stiffened Postbuckling Fuselage Panels - The effects of low energy impact on the structural integrity of two types of fuselage panels were evaluated: fuselage compression panels and fuselage shear panels.

Fuselage Compression Panels - Tests were performed to evaluate the effectiveness of Kevlar stitches for containing nonvisible low-energy impact damage in cocured skin-stiffener joints of buckled composite panels loaded in compression. Such damage nucleates disbonds which grow under cyclic loads and lead to panel failure. One method for containing disbonds and improving the durability of skin stiffener joints is to reinforce such joints with Kevlar stitches.

The baseline behavior of curved stiffened panels under compression postbuckling loads was determined in a previous test program (Reference 3). Fatigue failures were precipitated by local disbonds occurring in undamaged skin-stiffener joints.

Cyclic load tests were conducted on a curved stiffened panel identical to those previously tested except that each cocured joint was reinforced with two rows of Kevlar stitches. Low energy impacts were made to produce internal damage in two areas of high peel stress areas (Figure 32) where disbonds had occurred in the earlier cyclic load panel tests (Reference 3). The damage shown in Figure 32 (white areas of C-scan) was produced by a spherical indenter with 10 ft-lb impact energy.

Disbonds were detected and growth was monitored by periodic ultrasonic inspections. C-scan inspection records for the center stiffener of a baseline panel (3F) are shown in Figure 33, where sound attenuation occurring from disbonds and from air trapped within hat stiffeners is indicated by a black area. Disbonds in baseline panels initiated and grew from the base of the flange with increasing load cycles. An identical panel with stitching survived 1,000,000 cycles and showed only minor evidence of disbonding.

The damage containment capability of Kevlar stitches was significant. An unstitched, undamaged baseline panel suffered failure after 3,500 load cycles where the peak load was -55 kips. A stitched, undamaged panel was cyclically loaded without failure for 280,000 cycles to -50 kips followed by an additional 280,000 cycles to -55 kips. This test sequence using a stitched, damaged panel was repeated; again the reinforced panel survived both groups of 280,000 load cycles. In addition, ultrasonic inspections conducted after each block of 140,000 cycles indicated good containment of the impact damage with no disbond growth. Reinforcement with Kevlar stitches was, in this case, an effective means of assuring durability of cocured joints having nonvisible impact damage.

Fuselage Shear Panels - Tests were also performed to determine the effect of low energy impact damage on the static and fatigue strength of integrally stiffened shear-loaded panels operating in the postbuckling regime (Reference 4). The as-manufactured ultimate strength of the baseline test panel was 829 lb/in. A typical panel under postbuckling loads is shown in Figure 34. Maximum mid-panel lateral deflection for the static panels was in order of 0.2 inches.

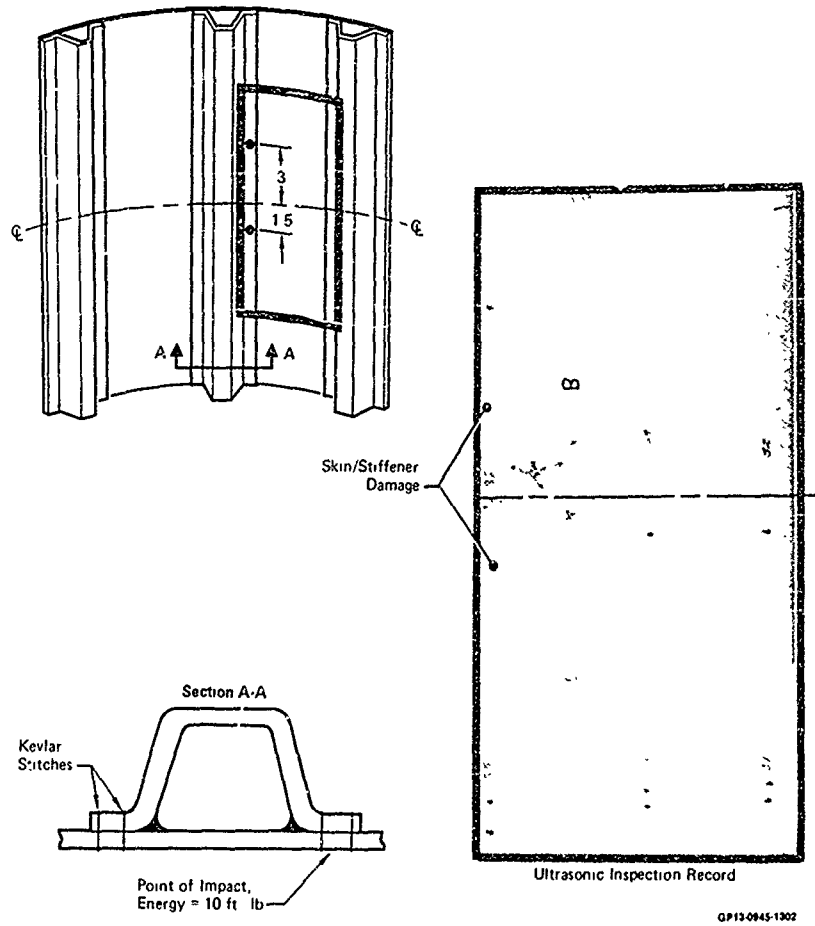
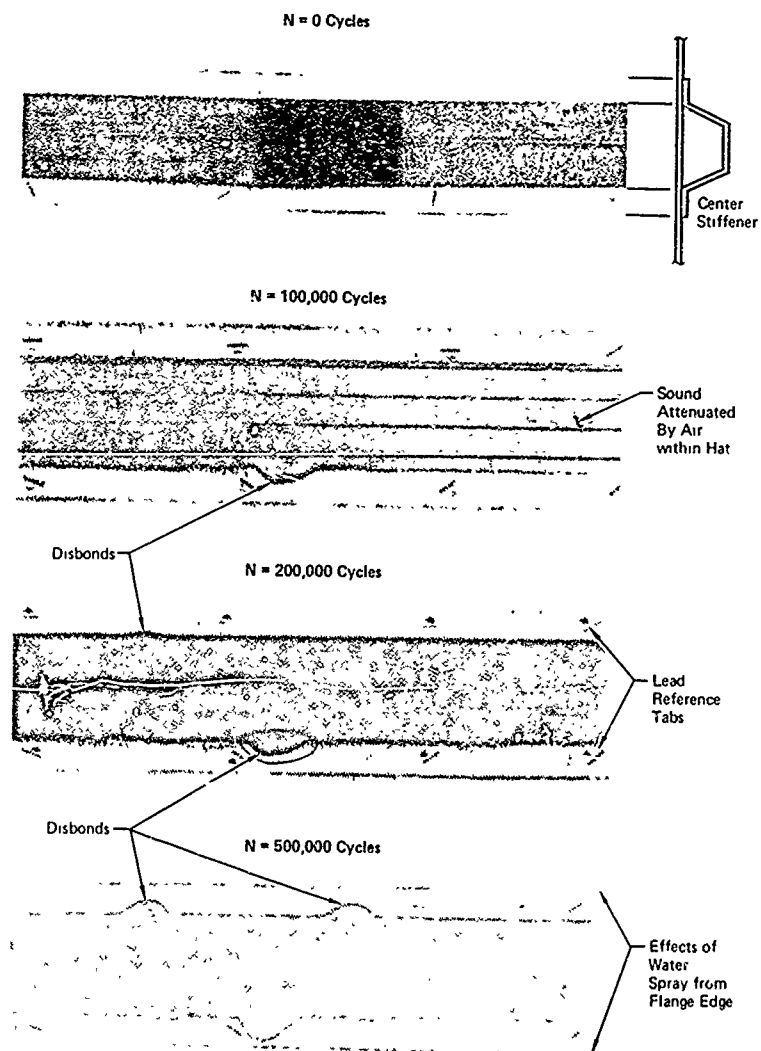


Figure 32. Damage Containment in Stitched Skin-to-Stiffener Joints



Baseline Panel 3F

OP15-0633-29

Figure 33. Growth of Disbonds in Flange-to-Skin Joint

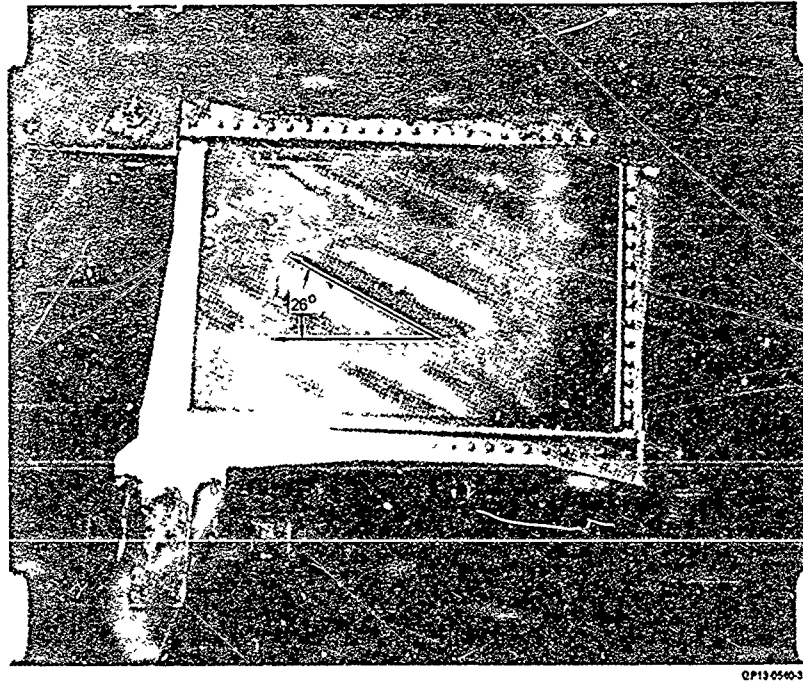


Figure 34. Buckled Shear Panel

The panel configuration and the locations of low energy impact damage is shown in Figure 35. An impact apparatus was designed with the capability of impacting the panels from either side. A slotted metal impact tube was used to direct the impact weight to the desired impact point. The 1/2 inch diameter round ball impact tool, Figure 36, rests against the panel and is centered inside the impact tube by a tool guide. All damaged panels were impacted on the skin side.

Panels were first impacted in the center bay using decreasing energy levels starting at 10 ft-lbs. The threshold level at which full penetration was achieved was in the range of 4.0 to 4.5 ft-lbs. Impact energy levels up to 4.0 ft-lbs have been estimated for fuselage lower surface for foreign object damage such as ice and gravel impacts during landing and take-off situations and for fuselage vertical sides and corners for ground handling impacts from hard objects such as tools (Reference 5).

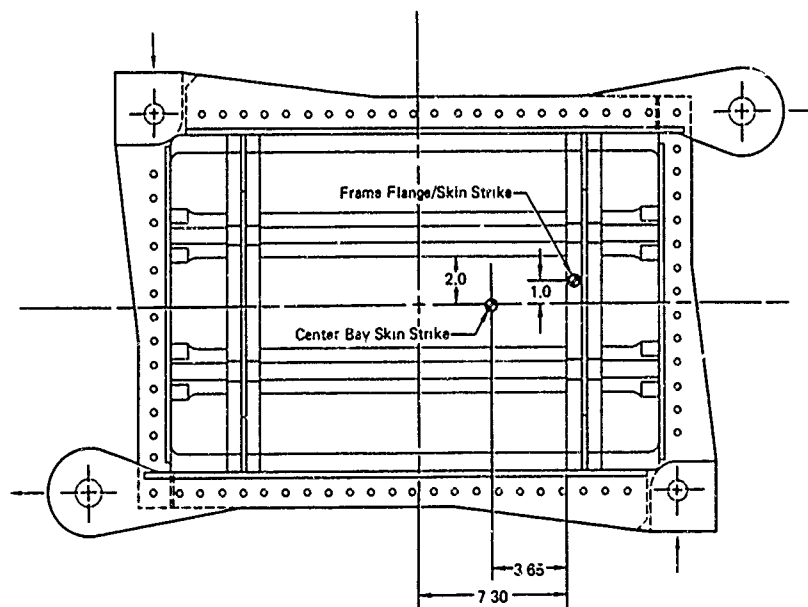
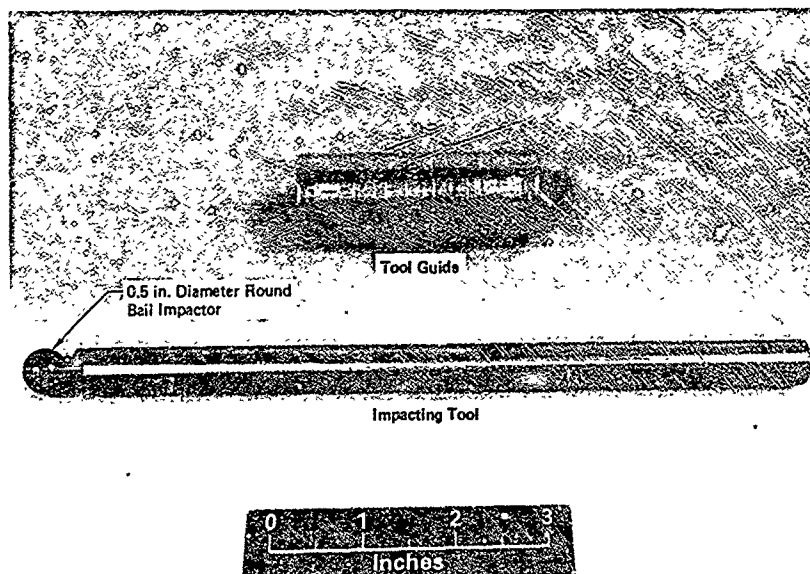


Figure 35. Shear Panel Configuration and Impact Damage Locations



GPC3 0726-28

Figure 38. Impacting Tool and Guide

A test panel after being subjected to multiple strikes in the range of 4.0 to 4.5 ft-lbs is shown in Figure 37. It was observed that while damage on the skin outer surface appeared different at different energy levels, the damage on the inner surface, in the form of delamination of the outer +45° ply, was similar for all strikes. A second impacted panel showed similar behavior.

Enhanced radiographic inspections of the strikes at 4.25 and 4.3 ft-lbs are shown in Figure 38. An energy level of 4.30 ft-lbs was adequate to achieve broken fibers across full 1/2 inch diameter. Internal damage was diamond shaped, probably due to 0, +45, 90 ply orientations. Through-the-thickness damage as indicated by radiographic inspection was similar for both energy levels, although visual appearances were different. Delamination on the inner surface of the skin (stiffener side) in the outer +45° ply extended to the adjacent hat flange (both sides).

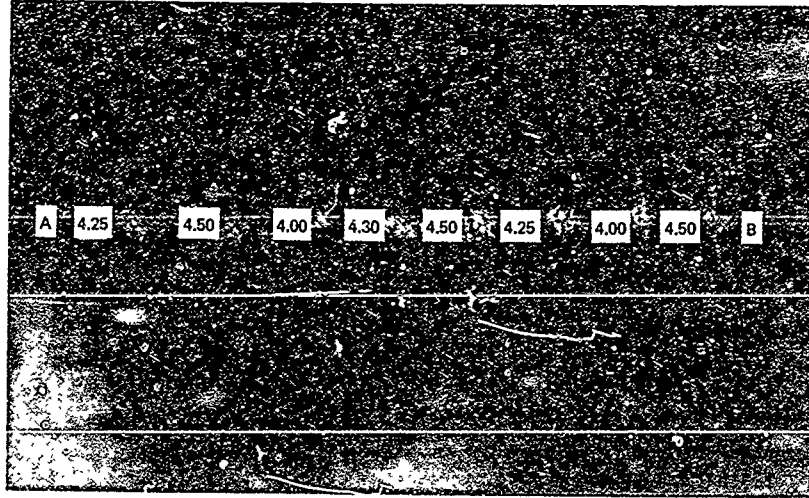
Five additional panels were damaged using an energy level of 4.30 ft-lbs. Three panels were impacted at a buckle crest location in the center bay of the panel. The remaining two panels were impacted at a location where failures occurred during fatigue loading of the baseline panels. These impact locations are shown in Figure 35. All panels were impacted on the skin side.

Of the three panels impacted in the center bay, one panel was statically tested to failure; the remaining two panels were fatigue tested at a load level to preclude stiffener disbonding. The two panels impacted at the critical stiffener/skin interface region were fatigue tested to a load which produced stiffener disbonding in the baseline panels.

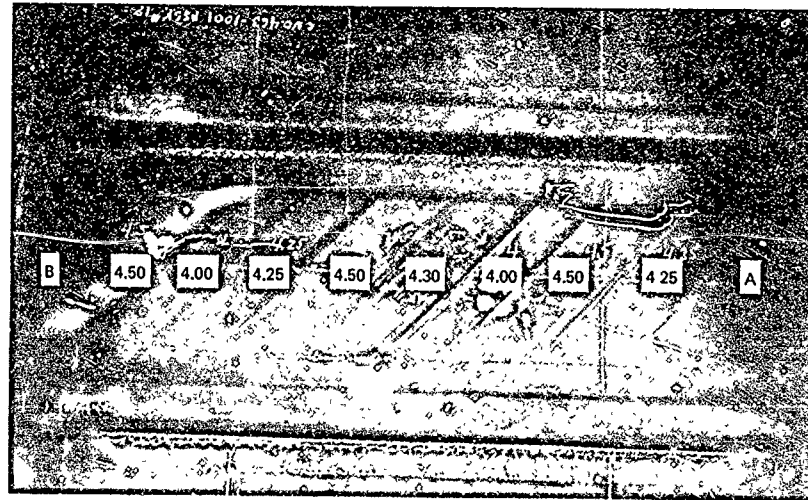
The damage sustained by the panel for static testing which was subjected to a center bay impact of 4.30 ft-lb is shown in Figure 39. The radiograph of this area is shown in Figure 40. The degree and type of damage was similar to that obtained in the exploratory tests.

Initial buckling for the impacted panel occurred at 104 lb/in and panel static failure occurred at 771 lb/in, compared to an average of 829 lb/in for the undamaged static test panels. Strain data was similar to data obtained in tests of undamaged panels; however, the maximum strain magnitudes achieved were less due to the lower failing load. This panel failed across the tension diagonal through the impacted region, preceded by stiffener separation similar to baseline static test panels.

The two fatigue test panels which were subjected to center bay impact damage were tested to a maximum fatigue load of 50% of ultimate strength ($N_{xymax} = 415$ lb/in). Previous tests showed this level to be the endurance limit of the as-manufactured panels.



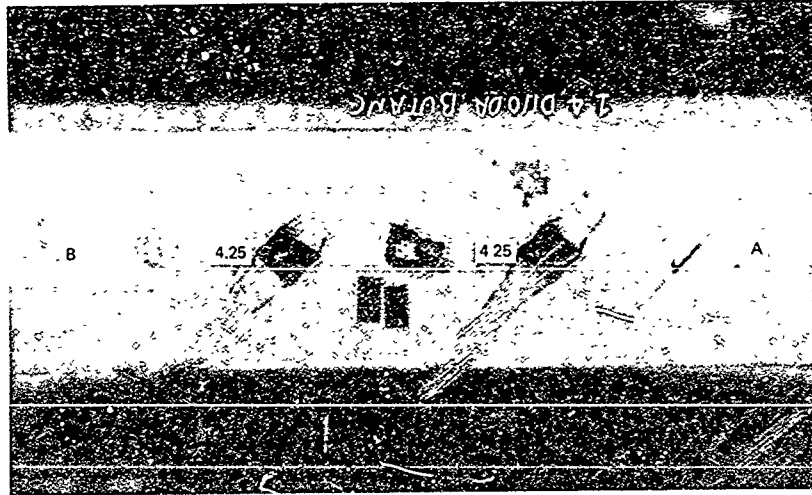
(a) Skin Side



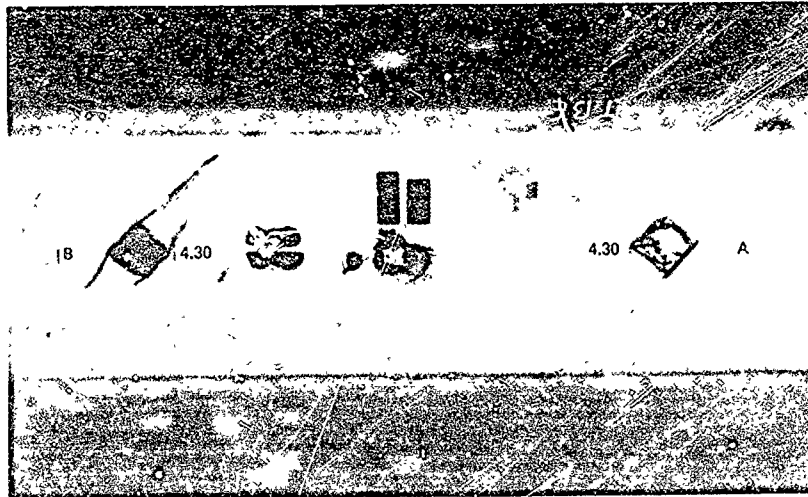
(b) Stiffener Side

GP03-0728-21

Figure 37. Impact Damage Investigation



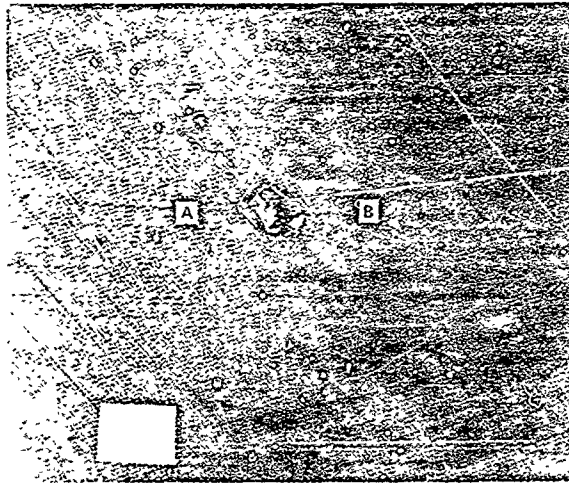
(a) 4.25 ft-lb



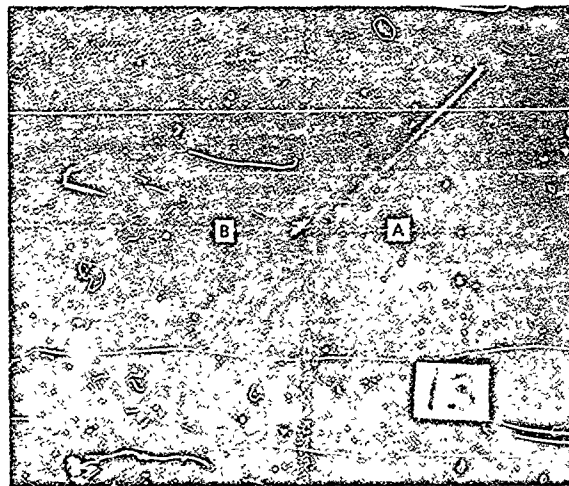
(b) 4.30 ft-lb

GP03-0728-26

Figure 38. Radiographic Inspection



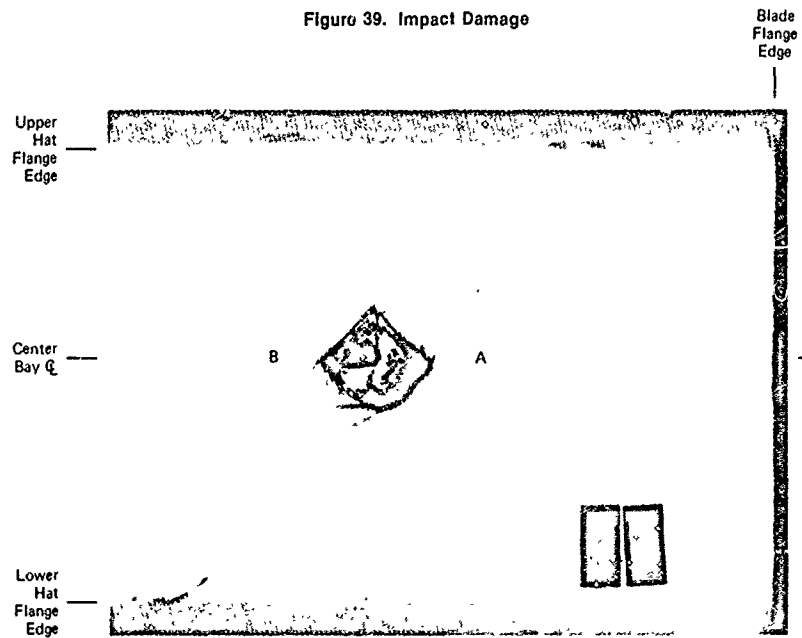
(a) Skin Side



(b) Stiffener Side

GPO-0728-23

Figure 39. Impact Damage



GPO30728-20

Figure 40. Radiographic Inspection of Impact Damage

All panels were subjected to constant amplitude fatigue loading at a stress ratio $R = 0.1$ for two blocks of 50,000 cycles each for a total of 100,000 cycles or failure, whichever occurred first. Strain surveys were taken prior to testing, and after each block of cycling to determine the effect of fatigue on panel performance. Panels surviving 100,000 cycles were subjected to a residual strength test. A summary of all fatigue results is presented in Figure 41 and in Figure 42.

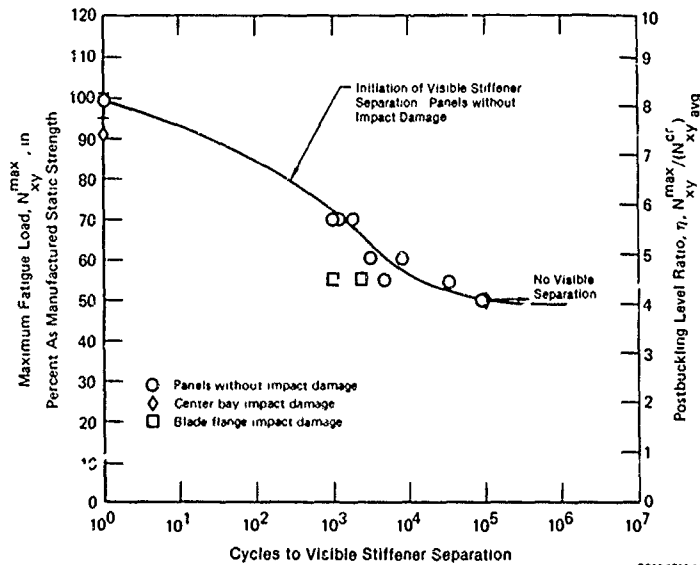
Panel	N_{xy}^{cr} 1 Cycle (lb/in.)	Static Strength (lb/in.)	N_{xy}^{max} Fatigue (lb/in.)	$\eta = \frac{N_{xy}^{max}}{(N_{xy}^{cr})^{avg}}$	Cycles to Visual Disbonding	Cycles Completed	N_{xy}^{cr} 50,000 Cycles (lb/in.)	N_{xy}^{cr} 100,000 Cycles (lb/in.)	Residual Static Strength (lb/in.)	Comments
1	98	851	-	-	1	1	-	-	-	As-Manufactured Static Test Panels
2	80	797	-	-	1	1	-	-		
3	93	838	-	-	1	1	-	-		
4	97	-	580	5.69	2,100	94,700	-	-	-	As-Manufactured Fatigue Test Panels
5	102	-	580	5.69	1,000	50,000	-	-	-	
6	96	-	580	5.69	1,200	50,000	-	-	849	
7	99	-	497	4.87	7,500	50,000	38	-	-	
8	108	-	497	4.87	3,000	50,000	48	-	-	
9	112	-	415	4.07	100,000+	100,000	112	112	947	
10	77	-	415	4.07	100,000+	100,000	30	30	973	
11	135	-	456	4.47	33,000	100,000	114	90	860	
12	78	-	456	4.47	4,500	100,000	48	48	890	
13	104	754	-	-	1	1	-	-	-	Impact Damage Center Bay Skin 1 Static Panel 2 Fatigue Panels
14	102	-	415	4.07	100,000+	100,000	102	96	858	
15	124	-	415	4.07	300 Δ	100,000	73	65	778	
16	115	-	456	4.47	950	100,000	63	54	918	Impact Damage Blade Flange/Skin 2 Fatigue Panels
17	120	-	456	4.47	2,300	100,000	77	77	861	

Δ Visual disbonding not observed after 100,000 cycles

GP03-0728-78

Δ Porosity noted prior to test

Figure 41. Summary of Test Results



GP03-0728-48

Figure 42. Panel Fatigue Performance

The impact damage sustained by the first fatigue test panel was similar to that observed both in the exploratory tests and in the static test panel. This panel survived 100,000 cycles with no visible stiffener separation or significant decrease in initial buckling strength observed. Radiographic inspections of the impact region prior to fatigue testing, after 50,000 cycles, and after 100,000 cycles are shown in Figures 43, 44, and 45 respectively. The damaged region did not grow during fatigue loading. Residual strength for the panel was 778 lb/in with sheet rupture occurring across the tension diagonal through the impacted region similar to that observed for the static test panel.

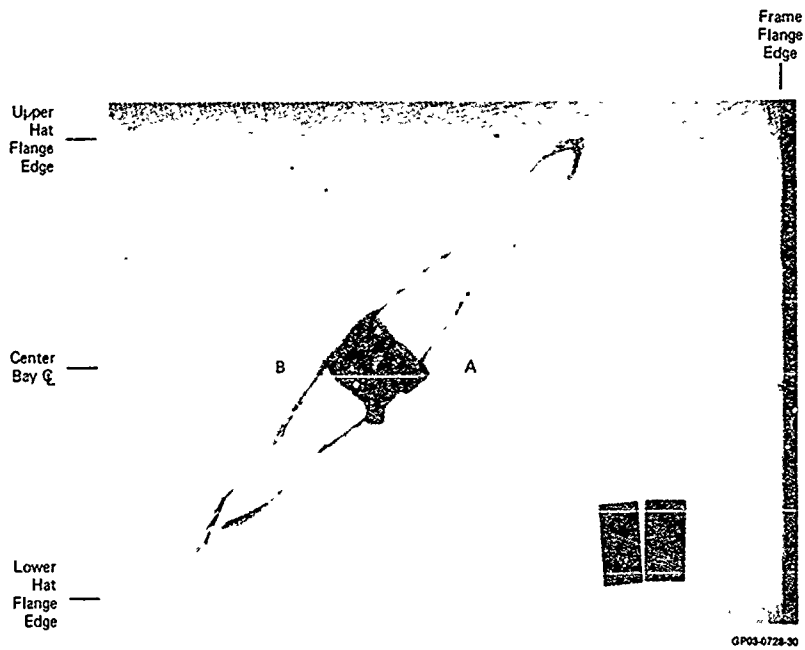


Figure 43. Radiographic Inspection of Initial Impact Damage

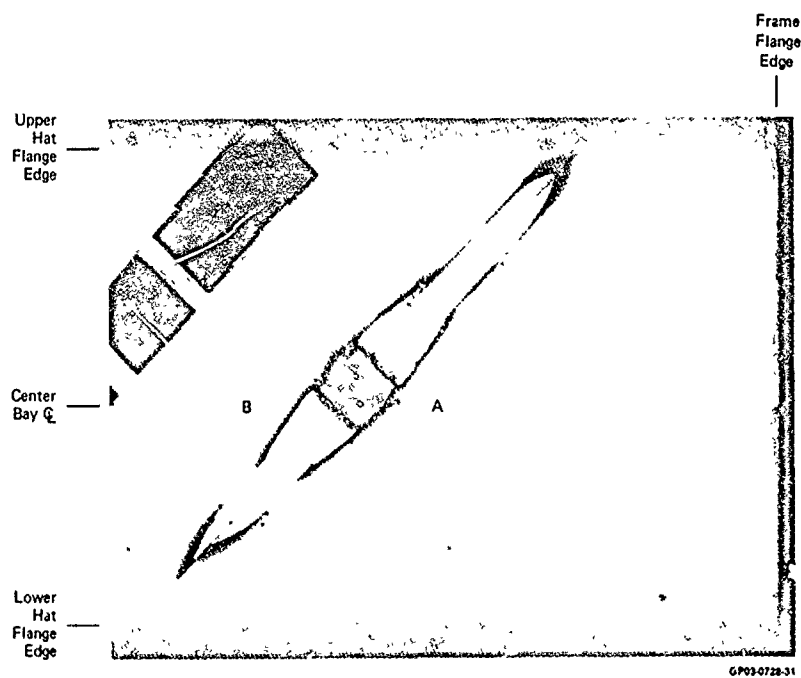


Figure 44. Radiographic Inspection of Impact Damage After 50,000 Cycles

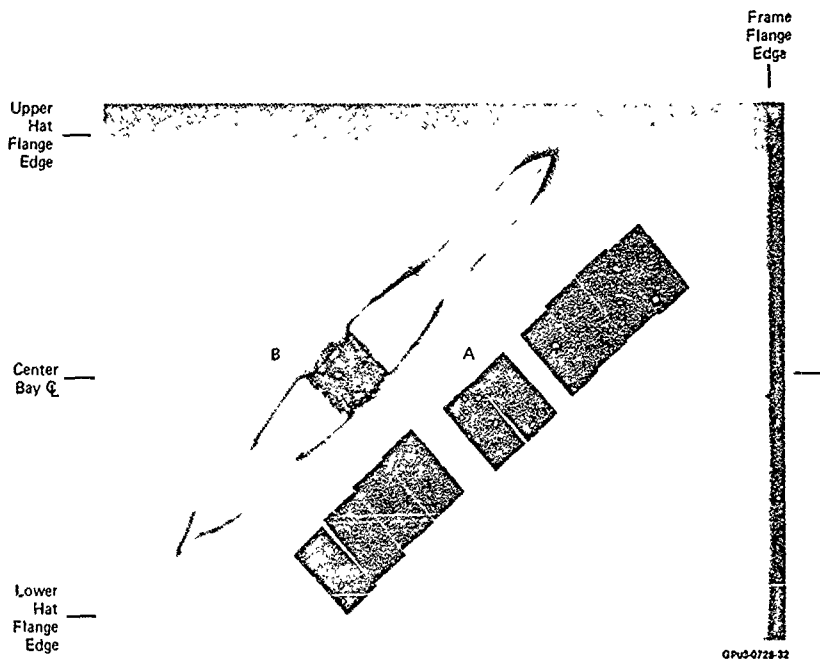


Figure 45. Radiographic Inspection of Impact Damage After 100,000 Cycles

Two other panels were impacted at the critical frame flange/skin location and subsequently fatigue tested. These panels were tested to a maximum fatigue load of 55% of ultimate strength to assure frame flange/skin separation. Both panels survived 100,000 cycles with visible stiffener separation occurring at the impact location at 950 and 2300 cycles respectively. Baseline panels tested to this level separated at 4500 and 33,000 cycles, respectively.

The frame flange/skin separation in the impacted region became extensive for both panels during the first 50,000 cycles. The frame flange along the impacted side of the center bay became nearly totally separated from the skin, causing a shift in the center bay buckling mode. Mid-panel strain response, Figure 46, indicated that the majority of separation occurred during the first 50,000 cycles causing a shift in buckling mode as indicated by the change in strain data for cycles 50,000 and 100,000. Buckling strengths of 115, 63, and 53 lb/in prior to fatigue testing and after 50,000 and 100,000 cycles, respectively, also indicate that the majority of damage occurred during the first 50,000 cycles. Residual strengths for both impacted panels was greater than the baseline panels, with sheet rupture across the tension diagonal.

4. BALLISTIC DAMAGE

Tests and analyses were performed to evaluate the effects of damage from impact of 23 mm high-explosive ballistic projectiles on the residual strength of composite structure incorporating various damage containment features. Various test setups were used to simulate air-to-air and ground-to-air ballistic threats to upper and lower wing skins. Good correlation was obtained between measured residual strengths and predictions made using the maximum strain failure criterion in conjunction with peak strains calculated about a hole in an orthotropic plate.

Carbon/epoxy specimens representative of monolithic wing skins and, for comparison, an aluminum specimen were damaged using 23 mm HEI projectiles. All specimens were flat, unstiffened plates.

Three damage containment features were incorporated in some composite specimens and evaluated relative to the performance of baseline composite specimens. These features, Figure 47, included parallel rows of Kevlar stitches, closely-spaced parallel rows of unbedded glass/epoxy buffer strips, and wider-spaced parallel rows of wide glass/epoxy buffer strips.

The stitched specimens utilized Kevlar thread having a breaking strength of 120 lbs and installed at four to six stitches per inch. Improved durability and damage containment were previously demonstrated in structures where cocured skin-to-substructure joints were reinforced with Kevlar stitches. In the specimens which incorporated glass/epoxy buffer strips, the 0° plies of graphite/epoxy were locally replaced, through the thickness, with 0° plies of glass/epoxy on either 3.5 inch centers or 13.5 inch centers.

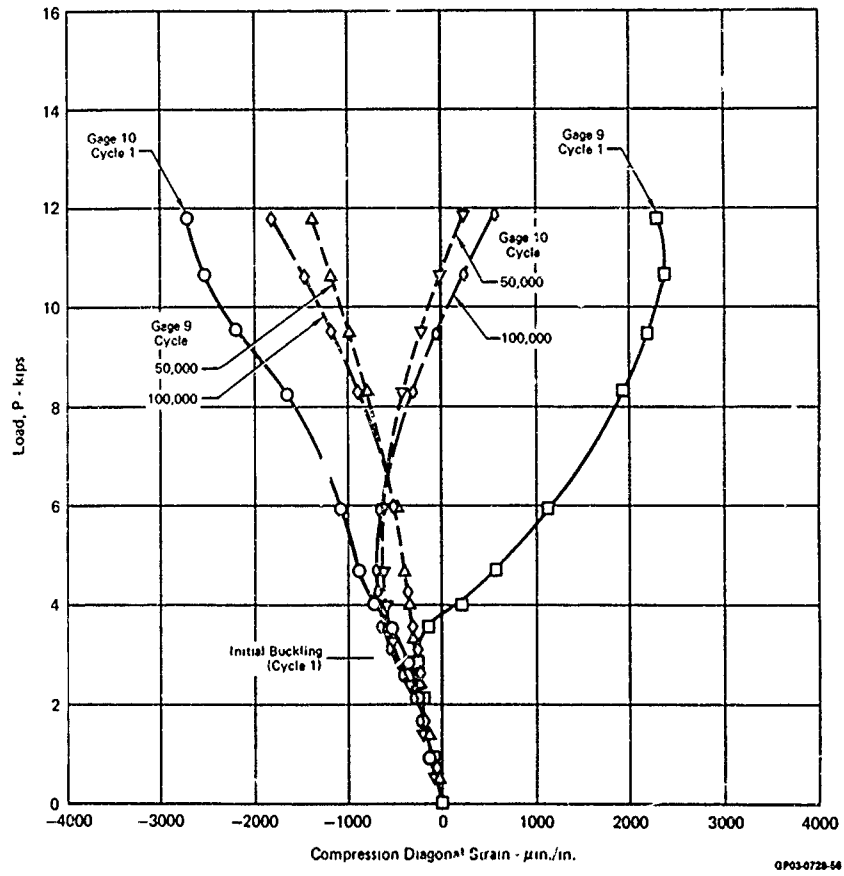
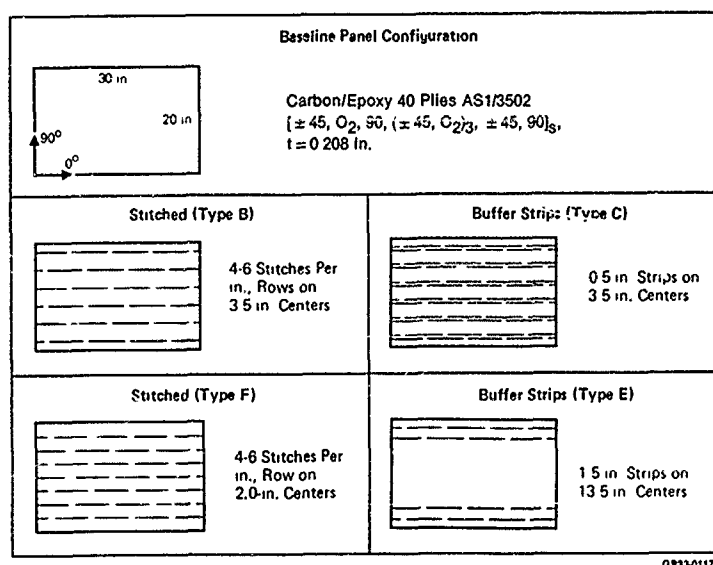
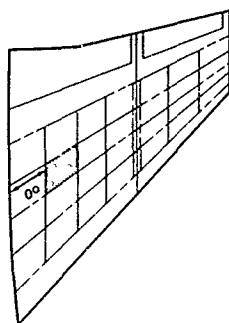


Figure 45. Mid-Panel Compression Diagonal Strains

OP03-0728-54



OP33-0117 21

Figure 47. Ballistic Test Specimens

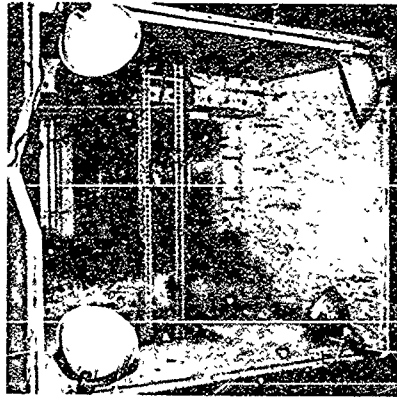
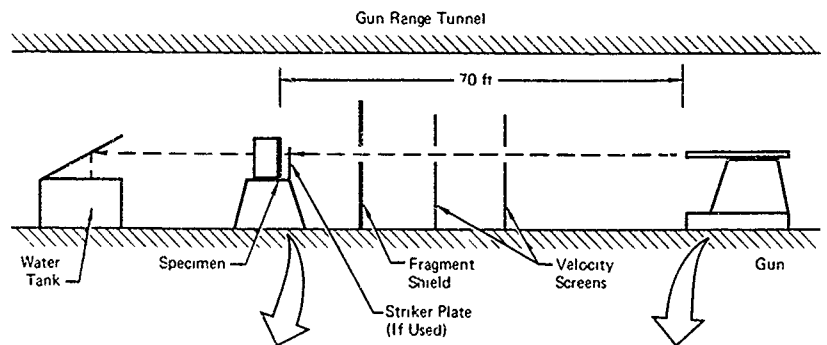
The test setup is shown in Figure 46. Projectile velocities, measured with photoelectric screens, ranged from 1773 fps to 1891 fps. The 23 mm projectile available for use in this program incorporated a "quick fuze" which was armed by inertial forces and, although triggered upon initial impact, featured a delay to allow 2-3 inch penetration prior to detonation. In this setup, the performance with a "superquick" fuze (instantaneous detonation) was simulated by positioning a striker plate in front of the specimen. Specimens were positioned normal to the trajectory. A water tank with deflector plate was used to capture fragments.

Damage from ballistic impact, Figure 49, ranged from a small, relatively clean, hole to a large diameter hole surrounded by delaminated plies, to a large multiple-penetration zone. Delay fuze projectiles penetrated the entrance-side skin, leaving the small hole shown in Figure 49(a), detonated in the wingbox, and sprayed fragments over a wide area of the exit-side skin, (Figure 49 (b)). Other projectiles, when a striker plate was positioned to simulate effects of superquick fuzes, led to the damage shown in Figure 50. Delaminated areas of test panels, detected in ultrasonic inspections, are identified by the dotted lines in Figures 49 and 50.

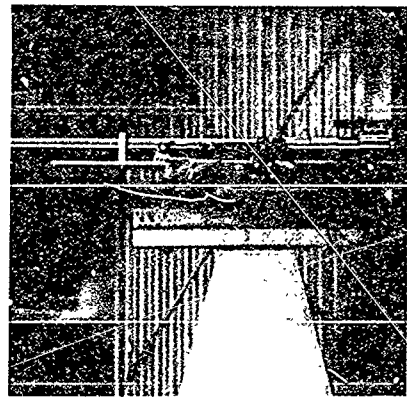
Ultrasonic inspection records presented in Figure 51 illustrate the extent of delamination in specimens incorporating the various containment features. Relative to baseline composite specimens, delaminations in stitched specimens were limited in width to the rows of stitches adjacent to the fragment-penetration hole. Ability of stitches to contain delaminations has been noted in other investigations. Damage in specimens incorporating buffer strips was also limited in width by the imbedded strips; however, some additional laminate damage was noted along the strips.

The relative behavior of carbon/epoxy and aluminum skins having the same flexural stiffness was also evaluated. The test setup was for simulating damage to the exit-side from a projectile with a delayed fuze. Test results are shown in Figure 52. The plasticity of the aluminum permitted to the blast/impact energy to be absorbed by permanent deformation of the metal. The composite specimen remained flat; however, it exhibited numerous penetrations and delaminations throughout the damage zone.

The residual tensile strength of damaged specimens was determined in room-temperature static tests and correlated with analytic predictions. Specimens with buffer strips, particularly the wider strips at spar locations, exhibited significant improvement in strength relative to baseline specimens. Stitching had no effect on residual strength.



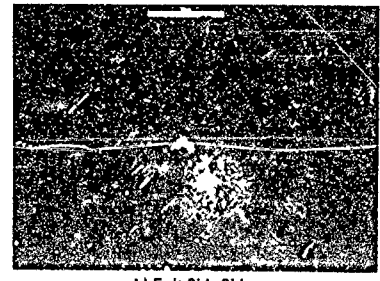
Specimen Installed with Striker Plate



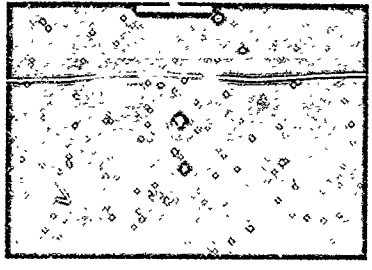
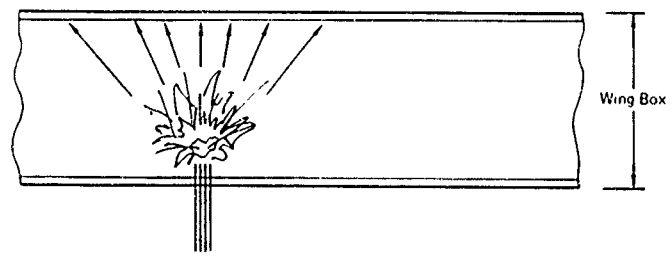
MCAIR 23 mm Gun

GP13-0945-1285

Figure 48. Ballistic Test Setup



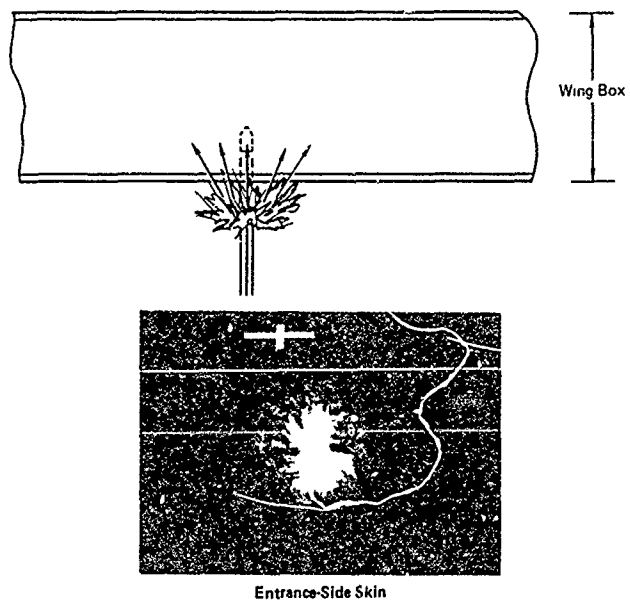
b) Exit-Side Skin



a) Entrance-Side Skin

GP13-0945 1272

Figure 49. Typical Ballistic Damage - Delayed Fuze Projectile



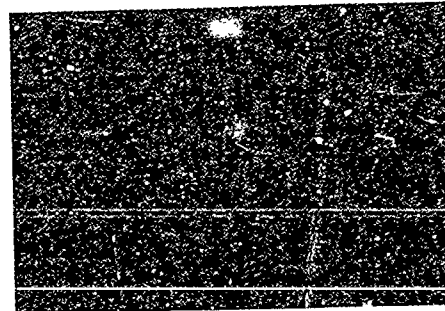
QP13 0945 1273

Figure 50. Typical Ballistic Damage - Superquick Fuze Projectile



QP330117 23

Figure 51. Delamination Damage Detected in Ultrasonic Inspections



a) Carbon/Epoxy Specimen



b) Aluminum Specimen

DP13-094-1284

Figure 52. Typical Damage of Composite Specimen Compared to Metal Specimen

Residual strengths are tabulated in Figure 53, along with the maximum visible damage and the maximum delamination damage detected by ultrasonics. Static failures were sudden with little time after failure initiation, except for those panels with buffer strips. Wide buffer strips stopped cracks from propagating across the width and turned the cracks lengthwise to propagate along the imbedded strips. Narrow, closely spaced buffer strips generally slowed to the propagation across the width. In general, use of buffer strips increased residual panel strength, except for specimens with a multi-penetration "shotgun blast" type of damage (Figure 49 (b)).

Residual tensile strengths are presented in Figure 54 as strain-to-failure for corresponding damage sizes. Strain-to-failure was calculated on the basis of the applied load at failure and gross-section properties. The range of damage presented for each specimen covers sizes from the maximum visible damage to the internal damage detected with ultrasonics. Specimens with buffer strips (shaded) exhibited significant improvement in residual strength relative to strength of baseline specimens (unshaded) having similar damage.

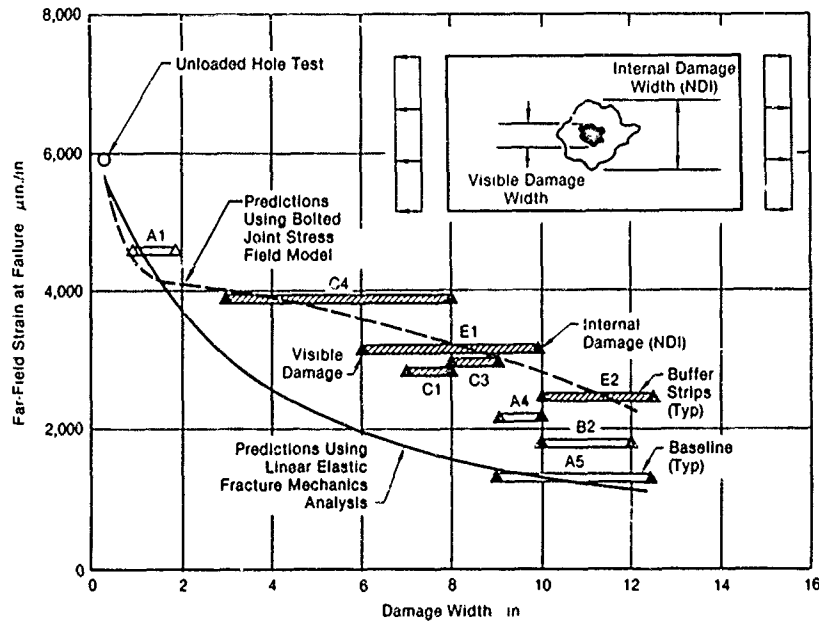
Specimen		Striker Plate Located to Simulate Damage for -	Measured Projectile Velocity (fps)	Visible Damage Diameter (in.)	Internal Damage Length (0°) x Width (90°) (in.)	Residual Tensile Strength (lb)
Type	ID					
Baseline Carbon/Epoxy	A1	Delayed Fuze, Entrance-Side Skin	1,891	1	2 x 2	180,250
	A2	Delayed Fuze, Exit-Side Skin	1,784	2		65,250
	A3	Superquick Fuze, Entrance-Side Skin	1,863	5	8 x 8	
	A4	Superquick Fuze, Entrance-Side Skin	1,863	9	14 x 10	84,000
	A5	Superquick Fuze, Entrance-Side Skin	1,870	9	14 x 14	50,600
Carbon/Epoxy with Rows of Stitches on 3.5-in Centers	B1	Superquick Fuze, Entrance-Side Skin	1,848	6	6 x 6	
	B2	Superquick Fuze, Entrance Side Skin	1,879	10	12 x 12	69,850
	B3	Delayed Fuze, Exit Side Skin	1,829	4		
	B4	Superquick Fuze, Entrance-Side Skin	1,826	6	8 x 8	
Carbon/Epoxy with 0.5-in Buffer Strips on 3.5-in Centers	C1	Superquick Fuze, Entrance-Side Skin	1,790	7	12 x 8	105,000
	C2	Delayed Fuze, Exit-Side Skin	1,880	2		74,200
	C3	Superquick Fuze, Entrance-Side Skin	1,787	8	16 x 9	107,500
	C4	Superquick Fuze, Entrance-Side Skin	1,862	3	16 x 8	143,250
Baseline Aluminum	D1	Delayed Fuze, Exit-Side Skin	1,859	4	-	
Carbon/Epoxy with 1.5-in Buffer Strips on 13.5-in Centers	E1	Superquick Fuze, Entrance Side Skin	1,865	6	10 x 10	115,000
	E2	Superquick Fuze, Entrance-Side Skin	1,864	10	16 x 13	89,500
Carbon/Epoxy with Rows of Stitches on 2.0-in Centers	F1	Superquick Fuze, Entrance-Side Skin	1,871	6	8 x 8	
	F2	Superquick Fuze, Entrance-Side Skin	1,854	7	9 x 11	

Notes

- ▲ Tests conducted as part of NADC contract N62269-80-C 0130
- ▲ Multiple penetrations over 20 in x 20 in area
- ▲ Structural tests not planned
- ▲ Permanent deformation over 16 in diameter with multiple penetrations
- ▲ Structural tests not complete

GP13-0645 1275

Figure 53. Test Results - Ballistically Damaged Specimens



GP13-0645 1276

Figure 54. Residual Strength of Ballistically-Damaged Specimens

Two analytical procedures for predicting residual strength were evaluated. All predicted strengths were corrected for a finite specimen width (20 in.). Linear elastic fracture mechanics analysis techniques (Reference 6) were used to predict a lower bound. Projectile damage was assumed to consist of through-the-thickness defects equal in width to the maximum visible and maximum internal damage.

In the second approach, the damage was assumed to be a circular hole in an orthotropic plate, and the methodology of Reference 7 was used to predict strain distributions about the hole. These strains were used in conjunction with the Maximum Strain Failure Criterion to predict far-field strain to failure as a function of damage (hole) size. Good correlation was first obtained between predictions and test results for a 0.25-inch-diameter fastener hole followed by extension of predictions to larger damage sizes. The residual strength of specimens with buffer strips compare well with these predictions.

5. CONCLUSIONS

Several conclusions were drawn from results of the programs described above.

First, it was concluded that manufacturing defects which produced the more significant strength reductions were easily found by current NDE techniques and would have been rejected or repaired by current acceptance criteria. Tolerances and controls being used in fabrication and assembly of composite aircraft structures are adequate to assure uniform strength and structural performance.

Second, the propagation of damage from low energy impact is dependent on type of loading and strain levels. The strength loss of the damaged laminate can be approximated on the basis of an "equivalent" round hole. The propagation under repeated loads is relatively slow and can be confined by relative simple reinforcement techniques such as stitching.

Third, the damage caused by 23mm HEI ballistic impact is more significant than LEID. The loss of laminates strength due to ballistic damage of a given size is greater than from LEID of the same apparent size. To reduce the strength loss, more significant reinforcement techniques such as buffer strips are required; stitching is not adequate.

REFERENCES

1. S. P. Garbo and J. M. Ogonowski, "Effect of Variances and Manufacturing Tolerances on the Design Strength and Life of Mechanically Fastened Composite Joints, "Contract F33615-77-C-3140, USAF RPT AFWAL-TR-81-3041, April 1981.
2. T. V. Hinkle and R. A. Garrett, "High Strain Composite Wing for Fighter/Attack Type Aircraft - Concept Validation", NADC-80146-60, September 1982.
3. T. V. Hinkle and R. A. Garrett, "Examination of Postbuckled Compression Behavior of Curved Panels", MCAIR/NASC Contract N00019-79-C-0204, MDC RPT A7264, August 1982.
4. M. P. Renieri and R. A. Garrett, "Postbuckling Fatigue Behavior of Flat Stiffened Graphite/Epoxy Panels Under Shear Loading" NADC Contract No2269-79-C-0463, RPT NADC-78137-60, July 82.
5. Butler, B.M., "Wing/Fuselage Critical Component Preliminary Design (Northrop)", AFFDL-TR-78-174, March 1979.
6. Avery, J.G. and Bradley, S.J., "Design Manual for Battle Damage Tolerant Fiber Composite Structures", NASC Contract N00019-80-C-0048. Boeing Report D180-26092-1, June 1980.
7. Ogonowski, J.M., "Effect of Variances and Manufacturing Tolerances on the Design Strength and Life of Mechanically Fastened Composite Joints: Volume 3-Bolted Joint Stress Field Model (BJSFM) Computer Program User's Manual", AFWAL-TR-81-3041, Volume 3, April 1981.

